

Editor and reviewer's comments in black, replies in blue.

Comments from Editor:

The reviewers are mostly satisfied with the technical aspects of the paper, but there are clearly some remaining presentation issues. Please go through the entire paper carefully and edit it for grammar, word-usage, clarity, etc., including but not limited to those issues identified by the reviewers.

The next iteration will be an editor-only review, i.e. it will not go back to the reviewers.

Answer:

We appreciate the comment. We have gone through the manuscript carefully and addressed the presentation issues.

Comments from Reviewer 2:

The paper is significantly improved. The authors have answered my concerns well although I do have some concern at the statement : " First, modelers do need the aircraft measurements to provide PDF distributions of vertical velocities (personal communications: Guangjun Zhang, Xiaohong Liu and Sungsu Park). " I completely agree modellers NEED pdfs of updrafts they need \*correct\* PDFs OR they need to know the shortfalls and applicability of these observations

so as to correctly validate output from GCMs. The last thing we want to be doing as observationalists is to be introducing new biases into models by using unrepresentative data.

To this end I would suggest a final pass of the paper and where you have a statement like on line 22: "The downdrafts are stronger ..." I suggest the insertion of "observed" so "The observed downdrafts are stronger". This caveats the dataset against observational issues. You do not know if all the updrafts in ICE-T were stronger than COPE all you know is what you observe.

The manuscript still contains many typographical errors, mainly in the corrections added. The Authors need to get a final edit done before submission

All in all the manuscript is now more honest to the data and is nearing a standard acceptable for publication.

Answer:

We appreciate the comment. We agree modelers need to know the shortfalls and applicability of observations, which have been pointed out in the manuscript.

We have gone through the manuscript carefully and addressed the presentation issues.

# 1 **Characteristics of Vertical Air Motion in Isolated Convective**

## 2 **Clouds**

3

4 **Jing Yang<sup>1</sup>, Zhien Wang<sup>1</sup>, Andrew J. Heymsfield<sup>2</sup> and Jeffrey R. French<sup>1</sup>**

5 [1] {Department of Atmospheric Science, University of Wyoming, Laramie, WY}

6 [2] {National Center for Atmospheric Research, Boulder, CO}

7 Correspondence to: Zhien Wang (zwang@uwyo.edu)

8

### 9 **Abstract**

10 The vertical velocity and air mass flux in isolated convective clouds are statistically analyzed  
11 using aircraft in-situ data collected from three field campaigns: High-Plains Cumulus (HiCu)  
12 conducted over the mid-latitude High Plains, CONvective Precipitation Experiment (COPE)  
13 conducted in a mid-latitude coastal area, and Ice in Clouds Experiment-Tropical (ICE-T)

14 conducted over a tropical ocean. ~~This study yields the following results. (1)~~[The results show](#)  
15 ~~Small~~[small](#)-scale updrafts and downdrafts (< 500 m in diameter) are frequently observed in the  
16 three field campaigns, and they make important contributions to the total air mass flux. ~~(2)~~The  
17 probability density functions (PDFs) and profiles of the [observed](#) vertical velocity are provided.

18 The PDFs are exponentially distributed. The updrafts generally strengthen with height.

19 Relatively strong updrafts (> 20 m s<sup>-1</sup>) were sampled in COPE and ICE-T. The [observed](#)

20 downdrafts are stronger in HiCu and COPE than in ICE-T. ~~(4)~~The PDFs of the air mass flux are  
21 exponentially distributed as well. The [observed](#) maximum air mass flux in updrafts is of the  
22 order  $10^4 \text{ kg m}^{-1} \text{ s}^{-1}$ . The [observed](#) air mass flux in the downdrafts is typically a few times  
23 smaller in magnitude than that in the updrafts. Since this study only deals with isolated  
24 convective clouds, and there are many limitations and sampling issues in aircraft in-situ  
25 measurements, more observations are needed to better explore the vertical air motion in  
26 convective clouds.

27

## 28 1. Introduction

29 Convective clouds are an important component of the global energy balance and water cycle  
30 because they dynamically couple the planetary boundary layer to the free troposphere through  
31 [the vertical transport of](#) ~~vertical~~ heat, moisture and mass ~~transport~~ (Arakawa, 2004; Heymsfield  
32 et al., 2010; Wang and Geerts, 2013). The vertical velocity determines the vertical transport of  
33 cloud condensate, the cloud top height, and the detrainment into anvils, which further  
34 ~~impact~~ [influences](#) the radiative balance (Del Genio et al., 2005). Vertical velocity also has [a](#)  
35 significant impact on ~~the~~ aerosol activation, droplet condensation and ice nucleation in  
36 convective clouds, which [in turn](#) ~~control the~~ [impacts](#) cloud life cycle and precipitation efficiency.

37 In order to reasonably simulate convective clouds, the vertical air velocity must be parameterized  
38 reliably in numerical weather prediction models (NWPMs) and global circulation models (GCMs)  
39 (Donner et al., 2001; Tonttila et al., 2011; Wang and Zhang, 2014). However, the complexity of  
40 the vertical velocity structure in convective clouds makes the parameterization non-  
41 straightforward (Wang and Zhang, 2014). Observations show that in most of ~~the~~ convective

42 clouds the vertical velocity is highly variable, and consequently the detailed structure of  
43 convection cannot be resolved in many models (Kollias et al., 2001; Tonttila et al., 2011).  
44 Additionally, using the same parameterization of vertical velocity for different grid resolutions  
45 may result in different cloud and precipitation properties (Khairoutdinov et al., 2009).  
46 Furthermore, poorly parameterized vertical velocity may result in large uncertainties in the  
47 microphysics; for instance, the cloud droplet concentration may be underestimated due to  
48 unresolved vertical velocity (Ivanova and Leighton, 2008). Vertical velocity simulated by  
49 models with horizontal resolutions ~~down to~~of a few hundred meters may be more realistic (e.g.  
50 Wu et al., 2009), but more observations are needed to evaluate this suggestion.

51 Aircraft in-situ measurement has been the most reliable tool enabling us to understand the  
52 vertical velocity in convective clouds and to develop the parameterizations for models. Early  
53 studies (e.g. Byers and Braham, 1949; Schmeter, 1969) observed strong updrafts and downdrafts  
54 in convective clouds; ~~however,~~ however, their results have a large ~~uncertainty~~uncertainties, because the  
55 aircrafts were not equipped with inertial navigation systems (LeMone and Zipser, 1980). In 1974,  
56 the Global Atmospheric Research Program (GARP) Atlantic Tropical Experiment (GATE) was  
57 conducted off the west coast of Africa, focusing on tropical maritime convections (Houze, 1981).  
58 A series of findings based on the aircraft data collected from the project ~~was~~were reported. For  
59 example, the accumulated probability density functions (PDFs) of vertical velocity and diameter  
60 of the convective cores are lognormally distributed. The updrafts and downdrafts in GATE  
61 (tropical maritime clouds) were only one half to one third as strong as those observed in the  
62 Thunderstorm Project (continental clouds) (LeMone and Zipser, 1980; Houze, 1981). These  
63 findings stimulated later statistical studies of the vertical velocity in convective clouds.  
64 Jorgensen et al. (1985) found that the accumulated PDFs of vertical velocity in intense

65 hurricanes were also ~~lognormal~~-distributed [lognormally](#) and the strength was similar to that in  
66 GATE, but the diameter of the convective region was larger. Studies of ~~the~~-convective clouds  
67 over Taiwan (Jorgensen and LeMone, 1989) and Australia (Lucas et al., 1994) showed a  
68 magnitude of vertical velocity similar to that in GATE. Although the results from the  
69 Thunderstorm Project are suspect, the significantly stronger drafts reveal the possible difference  
70 between continental and tropical maritime convective clouds. Lucas et al. (1994) suggested that  
71 ~~the~~-water loading and entrainment strongly reduce the strength of updrafts in maritime  
72 convections. However, this underestimation of the updraft intensity may be also due to ~~the~~  
73 sampling issues, e.g. penetrations were made outside the strongest cores (Heymnsfield et al.,  
74 2010).

75 There are a few more recent aircraft measurements (e.g. Igau et al, 1999; Anderson et al., 2005),  
76 but the data are still inadequate to fully characterize the vertical velocity in convective clouds. In  
77 most of these earlier papers, the defined draft or draft core required a diameter no smaller than  
78 500 m; this threshold excluded many narrow drafts with strong vertical velocity and air mass  
79 flux. In addition, the earlier studies used 1-Hz resolution data, which, [at typical aircraft flight](#)  
80 [speeds](#), can resolve only ~~the~~-vertical velocity structures larger than a few hundred meters, but the  
81 narrow drafts may be important to the total air mass flux exchange and cloud evolution.  
82 Furthermore, previous aircraft observations for continental convective clouds were based only on  
83 the Thunderstorm Project; ~~;~~ thus, ~~new~~-[additional](#) data are needed to study the difference between  
84 continental and maritime convections.

85 Remote sensing by means of, for example, wind profil[ing](#)~~ers and~~ radars is another technique  
86 ~~which~~-[that](#) has often been used in recent years for studying the vertical velocity in convective  
87 clouds (e.g. Kollias et al., 2001; Hogan et al., 2009; Giangrande et al., 2013; Schumacher et al.,

88 2015). Using profiler data, May and Rajopadhyaya (1999) analyzed the vertical velocity in deep  
89 convections near Darwin, Australia. They observed that the updraft intensified with height and  
90 that the maximum vertical velocity was greater than  $15 \text{ m s}^{-1}$ . Heymsfield et al. (2010) studied  
91 the vertical velocity in deep convection~~s~~ using an airborne nadir-viewing radar. Strong updrafts  
92 were observed over both continental and ocean areas, with the peak vertical velocity exceeding  
93  $15 \text{ m s}^{-1}$  in most of the cases and exceeding  $30 \text{ m s}^{-1}$  in a few cases. Zipser et al. (2006) used  
94 satellite measurements to find the most intense thunderstorms around the world; they applied a  
95 threshold updraft velocity greater than  $25 \text{ m s}^{-1}$  to identify intense convection. Collis et al. (2013)  
96 ~~provides~~provided statistics of updraft velocities for different convective cases near Darwin,  
97 Australia using retrievals from scanning Doppler radars and a multi\_f-frequency profiler. Airborne  
98 volumetric Doppler radars have also been used to study the dynamic structure of convective  
99 clouds (e.g. Jorgensen and Smull 1993; Hildebrand et al. 1996; Jorgensen et al. 2000). Remote  
100 sensing has the advantage of being able to measure the vertically velocity at different heights  
101 simultaneously (Tonttila et al., 2011), and some of the techniques can detect the strongest updraft  
102 cores in convective clouds (Heymsfield et al. 2010; Collis et al. 2013). Volumetric radars can  
103 also provide three-dimensional (3D) structure of air motion in convective clouds (Collis et al.  
104 2013; Nicol et al. 2015; Jorgensen et al. 2000). However, remote sensing measurements are not  
105 as accurate as aircraft measurements, because ~~many of the~~ many of the assumptions ~~that are~~ needed to  
106 account for the contribution of hydrometeor fall speed in the observed Doppler velocity in order  
107 to ultimately estimate air velocity. In addition, ground-based radars can rarely provide good  
108 measurements over oceans, and airborne cloud radars often suffer from the attenuation and non-  
109 Rayleigh scattering in convective clouds. Therefore, in-situ measurements are still necessary in

110 order to characterize the dynamics in convective clouds and to develop parameterizations for  
111 models.

112 The present study provides aircraft data analysis of ~~the~~ updrafts and downdrafts in mid-latitude  
113 continental, mid-latitude coastal, and tropical maritime convective clouds using the fast-response  
114 in-situ measurements collected from three field campaigns: the High-Plains Cumulus (HiCu)  
115 [project](#), the CONvective Precipitation Experiment (COPE) and the Ice in Clouds Experiment-  
116 Tropical (ICE-T). [All data used in this study were compiled for individual, isolated](#)  
117 [penetrations](#)~~All of the clouds used in this study, but some of them merged as they evolved.~~

118 Statistics of the vertical velocity and air mass flux are provided. The Wyoming Cloud Radar  
119 (WCR), onboard the aircraft, is used to identify the cloud top height, and high frequency (25-Hz)  
120 in-situ measurements of vertical velocity are used to generate the statistics. The major limitations  
121 of aircraft in-situ measurements are the aircraft maybe not able to sample the strongest ~~part of~~  
122 ~~convective cloudons~~[convective cores](#) due to safety concern, and it only provides the information  
123 of vertical air motion at single levels. These weaknesses need to be kept in mind in the following  
124 analyses. Section 2 describes the datasets and wind measuring systems. Section 3 presents the  
125 analysis method. Section 4 shows the results. Section 5 discusses the possible factors those  
126 interact with vertical air motions, and conclusions are given in Section 6.

127

## 128 **2. Dataset and instruments**

### 129 **2.1 Dataset**



130 The data used in the present study were collected from three field campaigns: HiCu, COPE and  
131 ICE-T. Vigorous convective clouds were penetrated during the three field campaigns, including  
132 mid-latitude continental, mid-latitude coastal, and tropical maritime convective clouds. These  
133 [cloud](#) penetrations provide good quality measurements for studying the microphysics and  
134 dynamics in the convective clouds, as well as the interactions between the clouds and the  
135 ambient air. The locations of the three field campaigns are shown in Fig. 1. Information  
136 regarding the penetrations used in this study is summarized in Table 1.

137 The HiCu project was conducted mainly in Arizona and Wyoming (Fig. 1) from the 18<sup>th</sup> of July  
138 to the 5<sup>th</sup> of August, 2002, and from the 7<sup>th</sup> of July to the 31<sup>st</sup> of August, 2003 to investigate the  
139 microphysics and dynamics in convective clouds over [the](#) mid-latitude High Plains. The  
140 University of Wyoming King Air (UWKA) was ~~operated as the platform~~[the aircraft platform](#)  
141 [used in this study project](#). In 2002 and 2003, 10 and 30 research flights were ~~made~~[conducted](#),  
142 respectively. In this study, the 2002 HiCu and 2003 HiCu are analyzed together because they  
143 were both conducted over the High Plains and the sample size of 2002 HiCu is relatively small.  
144 Fast-response in-situ instruments and the Wyoming Cloud Radar (WCR, Wang et al., 2012) were  
145 operated during the field campaign to measure the ambient environment, cloud dynamics and  
146 microphysics ~~as well as~~[and the](#) two-dimensional (2D) cloud structure. As shown in Table 1,  
147 penetrations in HiCu ~~were made~~[occurred](#) between 2 km and 10 km MSL. The sample size is  
148 relatively ~~good~~[large for penetrations](#) below 8 km and relatively small above 8 km. [Accumulated](#)  
149 [aircraft flight length in cloud was](#)~~The aircraft flew~~ about 2000 km~~in clouds~~. In-situ  
150 measurements and WCR worked well in these flights; however, the upward-pointing radar was  
151 operated in less than half of the research flights, and thus only a sub-set of the cloud ~~tops~~[top](#)  
152 [heights](#) can be estimated [from the observations](#). Fig. 2a(1–3) shows an example of the clouds

153 sampled in HiCu, including WCR reflectivity, Doppler velocity and 25-Hz in-situ measurement  
154 of the vertical velocity. In HiCu, both developing and mature convective clouds were penetrated;  
155 some penetrations were near cloud top, while most ~~of them~~ were more than 1 km below cloud  
156 top. The typical WCR reflectivity ~~is~~ ranges from 0 to -15 dBZ in the convective cores. In these  
157 clouds, reflectivity is strongly impacted by ~~due to strong~~ Mie scattering at the WCR wavelength.  
158 From the Doppler velocity and the in-situ vertical velocity, we ~~can~~ see that, in both the  
159 developing and mature cloud, relatively strong updrafts and downdrafts were observed, and  
160 multiple updrafts and downdrafts existed in the same cloud. These drafts maybe strong for  
161 isolated convections, but not ~~necessary~~ necessarily strong compared to the strongest updrafts in  
162 mesoscale convective systems (MCSs). No balloon soundings are available to measure the  
163 ambient environment in HiCu, so we ~~have to~~ use aircraft measurements to characterize the  
164 thermodynamic environment and estimate the convective available potential energy (CAPE). In  
165 some cases, the full CAPE cannot be calculated since the aircraft only flew at low levels ~~←~~  
166 (below 10 km MSL). The aircraft measurements suggest that the CAPE in HiCu ~~range~~  
167 less than  $100 \text{ J kg}^{-1}$  to more than  $500 \text{ J kg}^{-1}$ .

168 The COPE project was conducted from the 3<sup>rd</sup> of July to the 21<sup>st</sup> of August, 2013 in Southwest  
169 England (Fig. 1). The UWKA was used to study the microphysics and entrainment in mid-  
170 latitude coastal convective clouds (Leon et al., 2015). Seventeen research flights were  
171 conducted. The penetrations focused on regions near cloud top, which is verified based on the  
172 radar reflectivity from the onboard WCR. Since COPE was conducted in a coastal area, the  
173 convection initiation mechanism is different from that over a purely continental or ocean area. In  
174 addition, although the ambient air mainly came from the ocean, continental aerosols might be  
175 brought into the clouds, since many of the convective clouds formed within the boundary layer,

176 ~~which~~ further ~~affect~~impactings the microphysics and dynamics ~~in the~~of these clouds. ~~The~~  
177 ~~m~~MMeasurements ~~made in~~from COPE include temperature, vertical velocity, liquid water content,  
178 and particle concentration and size distributions. The WCR provided ~~excellent~~ measurements of  
179 reflectivity and Doppler velocity. The downward Wyoming Cloud Lidar (WCL) was operated to  
180 investigate the liquid (or ice) dominated clouds. The typical WCR reflectivity ~~is~~ranged from 5 to  
181 ~~-20~~ dBZ in the convective cores. Between 0 km and 6 km, there were about 800 penetrations  
182 ~~were made~~. Accumulated ~~f~~Flight distance in cloud totaled about 1000 km. The sample sizes are  
183 relatively ~~good~~large between 2 km and 6 km, but relatively small between 0 km and 2 km.  
184 Examples of the penetrations are given in Fig. 2b(1–3). COPE has fewer penetrations than HiCu,  
185 and most of the penetrations are near the cloud top. Fig. 2b(2) reveals relatively simple structures  
186 of the updrafts and downdrafts in COPE compared to HiCu, but as shown by the 25-Hz in-situ  
187 vertical velocity measurement in Fig. 2b(3), there are still many complicated fine structures in  
188 the vertical velocity distribution. The typical CAPE estimated from soundings in COPE was a  
189 few hundred J kg<sup>-1</sup>.

190 The ICE-T project was conducted from the 1<sup>st</sup> of July to the 30<sup>th</sup> of July, 2011 near St. Croix,  
191 U.S. Virgin Islands (Fig. 1), with state-of-the-art airborne in situ and remote sensing  
192 instrumentations, with the aim of studying the role of ice generation in tropical maritime  
193 convective clouds. The NSF/NCAR C-130 aircraft was used during ICE-T to penetrate  
194 convective clouds over the Caribbean Sea. Thirteen C-130 research flights were conducted  
195 during the field campaign, ~~with vigorous convective clouds penetrated~~. In-situ measurements  
196 from ICE-T include the liquid and total condensed water contents, temperatures, vertical  
197 velocities, and cloud and precipitating particle concentrations and size distributions. The WCR  
198 was operated on seven research flights to measure the 2D reflectivity and Doppler velocity fields.

199 ~~The~~ Typical WCR reflectivity ~~within the~~ convective cores ~~is ranged from~~ 10 to -20 dBZ. ~~The~~  
200 ~~Accumulated flight distance through clouds was~~ aircraft flew ~~more~~ greater than 1500 km ~~in~~  
201 ~~clouds,~~ through the ~~and~~ more than 650 ~~cloud~~ penetrations ~~were made~~ between 0 km and 8 km.  
202 The sample sizes are good except between 2 km and 4 km (Table 1). Examples of the  
203 penetrations are shown in Fig. 2c(1–3). During ICE-T, clouds in different stages were penetrated,  
204 including developing, mature and dissipating, some near cloud top and some considerably below  
205 cloud top. Maximum observed u ~~Updrafts up to were~~ 25 m s<sup>-1</sup>. ~~updrafts were observed, the~~  
206 ~~d~~ Downdrafts in ICE-T ~~are~~ were typically weaker than those in HiCu and COPE. The vertical  
207 velocity structures are complicated, as confirmed by both the Doppler velocity and the 25-Hz in-  
208 situ measurement. Weak updrafts and downdrafts were also observed in the dissipating clouds.  
209 The typical CAPE in ICE-T was greater than 2000 J kg<sup>-1</sup>, which is larger than that in HiCu and  
210 COPE.

211 During the sampling of isolated convective clouds in all the three field campaigns, ~~we typically~~  
212 ~~aligned the central part of cloud to penetrate at the flight height~~ the aircraft was typically aligned  
213 to penetrate through the center of the convective turret, ~~but still~~ however, ~~the aircrafts might not~~  
214 ~~penetrate through the strongest parts of convective cores due to safety concern~~ this does not  
215 guarantee that the aircraft always penetrated through the strongest updraft at that level. In  
216 addition, aircraft in-situ measurements only provide the information of vertical air motion at  
217 single levels. Moreover, the clouds sampled are isolated convective clouds, MCSs were not  
218 sampled. These limitations need to be kept in mind in interpreting the results from the following  
219 ~~analysis~~ analyses.

220

## 221 2.2 Wind measuring system

222 On both the C-130 and UWKA, a~~A Radome f~~Five-h~~Hole g~~Gust pProbe is installed for  
223 measurements of three-dimensional (3D) wind measurement. On the C-130, this probe is part of  
224 the fuselage radome, on the UWKA the probe is mounted on the end of an extended boom  
225 protruding from the front of the aircraft. In both cases~~A Radome Five Hole Gust Probe is an~~  
226 ~~aircraft radome~~ the probe with~~contains~~ five pressure ports installed in a “cross” pattern. Relative  
227 wind components (e.g. true air speed and flow angles) are sensed by a combination of  
228 differential pressure sensors attached to the five holes (Wendisch and Brenguier, 2013). Detailed  
229 calculation of relative wind components is described in Wendisch and Brenguier (2013). The  
230 time response and the accuracy of the pressure sensors is about 25 Hz and 0.1 mb. The 3D wind  
231 vectors ~~can be derived~~are determined by ~~taking out~~subtracting the aircraft  
232 ~~motion velocity~~velocitys from the relative wind measurement after rotating the vectors to a  
233 common coordinate system. On ~~both the~~ C-130 and UWKA, ~~the aircraft motion velocity~~velocity  
234 is ~~monitored~~measured by a Honeywell LASEREF SM Inertial Reference System (IRS), with an  
235 accuracy of 0.15 m s<sup>-1</sup> for vertical motion. Global Positioning System (GPS) was applied to  
236 remove the drift errors in the IRS position in all the three field campaigns (Khelif et al., 1998).  
237 The final vertical wind velocity product has an accuracy of about ±0.2 m s<sup>-1</sup>, and a time response  
238 of 25 Hz. This uncertainty (±0.2 m s<sup>-1</sup>) is a mean bias. For each output, the uncertainty is related  
239 to the true air speed, aircraft pitch angle, roll angle and ambient conditions. Therefore, the  
240 random error varies and could be larger than the mean bias. More information about the wind  
241 measurement on C-130 and UWKA can be found on the C-130 Investigator Handbook (available  
242 on <https://www.eol.ucar.edu/content/c-130-investigator-handbook>) and UWKA Investigator  
243 Handbook (available on [http://www.atmos.uwyo.edu/uwka/users/KA\\_InstList.pdf](http://www.atmos.uwyo.edu/uwka/users/KA_InstList.pdf))

244

### 245 3. Analysis method

#### 246 3.1 Identifying cloud using in-situ measurements

247 The Particle Measuring Systems (PMS) Two-Dimensional Cloud (2D-C) Probe and the Forward  
248 Scattering Spectrometer Probe (FSSP) are often used to characterize cloud microphysics (e.g.  
249 Anderson et al., 2005), although different thresholds of 2D-C and FSSP concentrations are  
250 usually used to identify the edge of a cloud. In this paper, we also use FSSP and 2D-C probes to  
251 find the cloud edges. In order to find a reasonable threshold for identifying cloudy air, we first  
252 use the WCR reflectivity to identify the clouds and the cloud-free atmosphere; for those regions  
253 we then plot the particle concentrations measured by FSSP and 2D-C in order to determine ~~the~~  
254 reasonable thresholds, and we apply the thresholds of particle concentrations to all the research  
255 flights without WCR.

256 To identify clouds using WCR, the six effective range gates nearest to the flight level (three  
257 above and three below) are chosen in each beam. Any beam in which the minimum reflectivity at  
258 the six gates exceeds  $-30 \text{ dBZ}^1$  is identified as in-cloud.

259 Fig. 3 shows the occurrence distribution as a function of the particle concentrations measured by  
260 FSSP versus the concentrations of the particles  $\geq 50 \mu\text{m}$  in diameter measured by 2D-C in the  
261 clouds identified by WCR reflectivity. From the figure, we ~~can~~ see that the FSSP concentration  
262 ranges from  $0.01 \text{ cm}^{-3}$  to  $1000 \text{ cm}^{-3}$ , and the 2D-C concentration ranges from  $0.1 \text{ L}^{-1}$  to  $10000 \text{ L}^{-1}$ .

---

<sup>1</sup> Based on the reflectivity measured in cloud-free air, the noise level of WCR reflectivity is  $-32 \text{ dBZ}$  at a range of 500 m and  $-28 \text{ dBZ}$  at a range of 1000 m. In this study, we choose  $-30 \text{ dBZ}$  as the threshold to identify cloud. This threshold ( $-30 \text{ dBZ}$ ) is examined for all three field campaigns.

263 Generally, shallow clouds have relatively higher concentrations of small particles and lower  
264 concentration of particles larger than 50  $\mu\text{m}$ . In deeper convective clouds, high concentrations  
265 can be seen for both small and large particles. The FSSP concentrations in cloud-free air are  
266 found to be  $2\text{ cm}^{-3}$  at most, and the FSSP concentrations measured below the lifting condensation  
267 level (LCL), where ~~precipitating~~ precipitation particles dominated, are lower than  $2\text{ cm}^{-3}$ ; as well.  
268 Therefore,  $2\text{ cm}^{-3}$  is selected as the concentration threshold to identify clouds based on the FSSP  
269 measurements, ~~as shown~~ indicated by the dashed line in Fig. 3. However, in some clouds (e.g.  
270 pure ice clouds), the FSSP concentration could be lower than  $2\text{ cm}^{-3}$ , and 2D-C concentrations  
271 are needed to identify these cold clouds. We chose a concentration of  $1\text{ L}^{-1}$  2D-C ~~concentration~~  
272 ~~for~~ particles with diameters larger than  $\geq 50\text{ }\mu\text{m}$  as the second threshold to identify cloud, ~~as~~  
273 ~~shown~~ indicated by the dotted line in Fig. 3. In order to avoid precipitating regions (below the  
274 LCL calculated from soundings), the second threshold is only applied to penetrations at  
275 temperatures colder than  $0\text{ }^{\circ}\text{C}$ ; ~~;~~ ; thus the cloud is defined ~~as~~ when FSSP concentration  $\geq 2\text{ cm}^{-3}$  or  
276 2D-C concentration  $\geq 1\text{ L}^{-1}$ . At temperatures warmer than  $0\text{ }^{\circ}\text{C}$ , the FSSP concentrations in most  
277 ~~of the~~ convective clouds are higher than  $2\text{ cm}^{-3}$ , so only the first threshold is used.

278 Once a cloud is identified, the penetration details can be calculated, including the flight length,  
279 the flight height, the cloud top height if WCR ~~data is~~ were ~~as~~ available, and the penetration  
280 diameter. The penetration diameter is calculated as the distance between the entrance and exit of  
281 a penetration. In order to reject ~~whirling penetrations and~~ penetrations with significant turns, we  
282 require that the diameter of a penetration be at least 90% of the flight length, so the cloud scale  
283 will not be significantly overestimated. ~~;~~ Since the aircraft might not penetrate exactly through the  
284 center of a cloud, the actual cloud diameter may be larger than the penetration diameter. Based  
285 on WCR reflectivity images, there are no isolated convective clouds sampled larger than 20 km

286 in diameter. There are a few penetrations longer than 20 km, but these clouds are more like part  
287 of MCSs, and so they are excluded from this study.

288

### 289 3.2 Defining updraft and downdraft

290 In previous studies of the vertical velocity based on in-situ measurements, the updraft and  
291 downdraft ~~are~~were often defined as an ascending or subsiding air parcel with the vertical  
292 velocity continuously  $\geq 0$  m s<sup>-1</sup> in magnitude and  $\geq 500$  m in diameter (e.g. LeMone and Zipser,  
293 1980; Jorgensen and LeMone, 1989; Lucas et al., 1994; Igau et al., 1999). In this study, we use a  
294 vertical velocity threshold of 0.2 m s<sup>-1</sup>, that is, the draft has a vertical velocity continuously  $\geq 0.2$   
295 m s<sup>-1</sup> in magnitude, because  $\pm 0.2$  m s<sup>-1</sup> is the accuracy of the instrument. Any very narrow and  
296 weak portion (diameter  $< 10$  m and maximum vertical velocity  $< 0.2$  m s<sup>-1</sup> in magnitude)  
297 between two relatively strong portions is ignored, and the two strong portions are considered as  
298 one draft.

299 The diameter threshold (500 m) is not used in this paper, because drafts narrower than 500 m  
300 frequently occur and they may make important contributions to the total air mass flux in the  
301 atmosphere and therefore they are necessarily to be considered in model simulations. Fig. 4  
302 shows the PDFs of the diameters of all the updrafts and downdrafts sampled in HiCu, COPE and  
303 ICE-T. In all the panels, the diameters are exponentially distributed, the PDFs can be fitted using

$$304 \quad f = \alpha \cdot |x|^\beta \cdot \exp(\gamma|x|) \quad (1)$$

305 where  $f$  is the frequency and  $x$  is the diameter. The coefficients  $\alpha$ ,  $\beta$  and  $\gamma$  for each PDF is shown  
306 in each panel. This function will also be used to fit the PDFs of vertical velocity and air mass



307 flux in the following analyses. Generally, as seen in Fig. 4, the PDFs broaden with [increasing](#)  
308 height ~~increases~~ for the three field campaigns; ~~this is~~ consistent with previous findings  
309 (LeMone and Zipser, 1980). The diameters of the [observed](#) updrafts are smaller in COPE  
310 compared to those sampled in HiCu and ICE-T, possibly because most of the penetrations are  
311 near cloud top. As shown in Fig. 4, many narrow drafts are observed. More than 85%, 90% and  
312 74% of the [observed](#) updrafts are narrower than 500 m (dotted lines) in HiCu, COPE and ICE-T,  
313 respectively, and more than 90% of the [observed](#) downdrafts in all three field campaigns are  
314 narrower than 500 m. A threshold of 500 m in diameter would exclude many small-scale drafts,  
315 therefore, in this study all the drafts broader than 50 m (dashed lines) are included. ~~The d~~Drafts  
316 narrower than 50 m are excluded because most of them are turbulence.

317 Fig. 5a shows the occurrence distributions as a function of the mean vertical velocity versus the  
318 diameter of the drafts with the vertical velocity continuously  $\geq 0.2 \text{ m s}^{-1}$  in magnitude. From the  
319 figure, it is noted that many drafts narrower than 500 m have quite strong vertical velocities. The  
320 maximum mean vertical velocity of these narrow drafts can reach  $8 \text{ m s}^{-1}$ , and the minimum  
321 mean vertical velocity in the downdrafts is  $-6 \text{ m s}^{-1}$ . With such strong mean vertical velocity,  
322 narrow drafts could contribute noticeably to the total air mass flux. Fig. 5b presents the  
323 occurrence distributions as a function of the air mass flux versus the diameter of the drafts. The  
324 air mass flux is calculated as  $\bar{\rho}\bar{w}D$  (LeMone and Zipser, 1980), where  $\bar{\rho}$  is the mean air density  
325 at the measurement temperature,  $\bar{w}$  is the mean vertical velocity and  $D$  is the diameter of each  
326 draft. Due to the limitation of aircraft [in-situ](#) measurements, the air mass flux is calculated using  
327 the data from ~~single~~-[single](#)-line penetrations. This may introduce additional uncertainties in air  
328 mass flux estimations for these clouds. Fig. 5b shows that the air mass flux in many drafts  
329 narrower than 500 m is actually larger than ~~that~~ [air mass flux](#) in some of the broader drafts. The

330 maximum value for these narrow updrafts reaches  $4000 \text{ kg m}^{-1} \text{ s}^{-1}$ , and the minimum value for  
331 the downdrafts reaches  $-3000 \text{ kg m}^{-1} \text{ s}^{-1}$ . The normalized accumulated flux (red curves) reveals  
332 that the drafts narrower than 500 m (dotted horizontal lines) ~~make very significant~~  
333 ~~contributions~~ contribute significantly to the total air mass flux. Calculations indicate  
334 that the updrafts narrower than 500 m contribute 20%–35% of the total upward flux, and that the  
335 downdrafts narrower than 500 m contribute 50%–65% of the total downward air mass flux.  
336 Drafts narrower than 50 m (dashed horizontal lines), which are excluded in this paper,  
337 contributes less than 5% of the total air mass flux.

338 In this study, we delineate three different groups of updrafts and downdrafts using three  
339 thresholds of air mass flux:  $10 \text{ kg m}^{-1} \text{ s}^{-1}$ ,  $100 \text{ kg m}^{-1} \text{ s}^{-1}$  and  $500 \text{ kg m}^{-1} \text{ s}^{-1}$  in magnitude. The air  
340 mass flux is used here to delineate the draft intensity because (1) air mass flux contains the  
341 information of both vertical velocity and draft size; (2) air mass flux can reveal the vertical mass  
342 transport through convection; and (3) air mass flux is an important component in cumulus and  
343 convection parameterizations (e.g. Tiedtke, 1989; Bechtold et al., 2001). The first designated  
344 group, the “weak draft,” with air mass flux  $10\text{--}100 \text{ kg m}^{-1} \text{ s}^{-1}$  in magnitude, contributes 10% of  
345 the total upward air mass flux and 10% of the total downward air mass flux. The “moderate  
346 draft,” with air mass flux  $100\text{--}500 \text{ kg m}^{-1} \text{ s}^{-1}$  in magnitude, contributes 25% of the total upward  
347 air mass flux and 40% of the total downward air mass flux. The “strong draft,” where the air  
348 mass flux  $\geq 500 \text{ kg m}^{-1} \text{ s}^{-1}$  in magnitude contributes 60% of the total upward air mass flux and 20%  
349 of the total downward air mass flux. The definitions of “weak”, “moderate” and “strong” only  
350 apply for the isolated convective clouds analyzed in this study, and are not necessarily  
351 appropriate for ~~other-organized~~ convections (e.g. MCS). Drafts weaker than  $10 \text{ kg m}^{-1} \text{ s}^{-1}$  are not  
352 analyzed because they are too weak and most of them are very narrow (Fig. 5b). The numbers of

353 weak, moderate and strong updrafts and downdrafts sampled at 0–2 km, 2–4 km, 4–6 km, 6–8  
354 km and 8–10 km MSL are shown in Table 2. Generally, weak and moderate drafts are more  
355 often observed than strong drafts. At most of the height ranges, more updrafts are observed than  
356 downdrafts.

357 Some researchers have defined a “draft core” by selecting the strongest portion [within](#) a draft.  
358 For example, LeMone and Zipser (1980) define an updraft core as an ascending air motion with  
359 vertical velocity continuously  $\geq 1 \text{ m s}^{-1}$  and diameter  $\geq 500 \text{ m}$ . This definition of a “draft core” is  
360 followed in a few more recent studies (e.g. Jorgensen and LeMone, 1989; Lucas et al., 1994;  
361 Igau et al., 1999). We too analyzed the vertical air motion characteristics in the stronger portion  
362 of the drafts considered here. However, we found that in many updrafts the strong portion where  
363 the vertical velocity is continuously  $\geq 1 \text{ m s}^{-1}$  dominates and contributes 80% of the total air  
364 mass flux, so the statistics of the vertical air motion characteristics in the stronger portion are  
365 very similar to those in the draft as a whole. Therefore, the present study focuses on “drafts” in  
366 which both weak and strong portions are included.

367

## 368 **4. Results**

### 369 **4.1 Significance of drafts in different strengths**

370 From the analysis above, we note that relatively small and weak updrafts are frequently observed  
371 in convective clouds. In this section, we provide further evidence to show the importance of the  
372 relatively weak updrafts in terms of air mass flux.

373 Fig. 6a shows the average number of updrafts as a function of air mass flux observed in the three  
374 field campaigns. The solid, dashed and dotted lines represent the penetrations with different  
375 diameters. As shown in Fig. 6a, weak and moderate updrafts are more often observed than strong  
376 updrafts, and ~~the numbers~~more of updrafts are ~~higher~~observed in longer penetrations. Since this  
377 is an average result, the number of updrafts could be smaller than 1 (e.g. many ~~narrow~~short  
378 penetrations do not have strong updrafts). Fig. 6b is similar to Fig. 6a but shows the occurrence  
379 frequency of updrafts with different air mass fluxes (i.e. the vertical axis in Fig. 6a is  
380 normalized). For the penetrations ~~<~~less than 1 km in length, many of the clouds only have weak  
381 or moderate updrafts, and relatively strong updrafts are rarely observed. For penetrations of 1–10  
382 km, the frequency of strong updrafts increases and the frequency of weak and moderate updrafts  
383 decreases. For even longer penetrations (>10 km), however, the frequency of weak updrafts  
384 increases again, indicating the increasing importance of weak updrafts.

385 Fig. 7 shows the average percentile contributions to the total upward air mass flux by the three  
386 different groups of updrafts as a function of penetration diameter. In Fig. 7a, all the penetrations  
387 are included. Since many narrow clouds have no strong updrafts in terms of air mass flux, the  
388 total air mass flux in these narrow clouds is mostly contributed by weak (red bar) and moderate  
389 (green bar) drafts. These narrow clouds may have a ~~high~~large vertical velocity but small air  
390 mass flux. As the diameter increases to 4 km, the contributions to total air mass flux from  
391 relatively weak updrafts (red bar) decrease, while those from stronger updrafts (blue bar)  
392 increase. For a penetration of 4 km length, 80%–90% of the total upward mass flux is  
393 contributed by the strong updrafts with air mass flux  $\geq 500 \text{ kg m}^{-1} \text{ s}^{-1}$ . However, for the  
394 penetrations with diameter larger than 4 km, the contribution from relatively weak updrafts  
395 increases, probably because more weak updrafts exist in wider clouds (Fig. 6). This is more

396 obvious in Fig. 7b, in which only the penetrations with at least one strong updraft are included.  
397 As the diameter increases from 400 m to 20 km, the contribution from the weak and moderate  
398 updrafts (red bars and green bars) increases from 2% to 20%. This suggests that as the cloud  
399 evolves and becomes broader (e.g. mature or dissipating stage), the weak and moderate updrafts  
400 are also important and therefore necessary to be considered in model simulations.

401

## 402 4.2 PDFs of vertical velocity and air mass flux

403 Fig. 8 shows the PDFs of the vertical velocity in the drafts sampled at 0–2 km, 2–4 km, 4–6 km  
404 and higher than 6 km in the three field campaigns. Columns (a), (b) and (c) represent the drafts  
405 with air mass flux  $\geq 10 \text{ kg m}^{-1} \text{ s}^{-1}$ ,  $\geq 100 \text{ kg m}^{-1} \text{ s}^{-1}$  and  $\geq 500 \text{ kg m}^{-1} \text{ s}^{-1}$  in magnitude,  
406 respectively; in other words, column (a) includes all the weak, moderate and strong of drafts,  
407 column (b) includes moderate and strong updrafts, and column (c) includes strong updrafts only.  
408 For statistical analysis, it is better to analyze different drafts together rather than separately.

409 Since the aircraft might under-sample the strongest updraft cores, the tails of [the](#) PDFs could  
410 [be](#) biased low, but these PDFs still provide valuable information. In all the panels, the [observed](#)  
411 vertical velocities are exponentially distributed for both updrafts and downdrafts; the PDFs can  
412 be fitted using Eq. (1). From Fig. 8 we ~~can~~ see that at 0–2 km, the PDFs for both COPE and ICE-  
413 T are narrow. At 2–4 km, stronger updrafts and broader PDFs are observed in both COPE and  
414 ICE-T compared to those at 0–2 km, ~~and~~ [the](#) maximum vertical velocity is about  $15 \text{ m s}^{-1}$ . In  
415 COPE, the [observed](#) downdrafts are stronger than those in ICE-T, with the minimum vertical  
416 velocity as low as  $-10 \text{ m s}^{-1}$ . For HiCu, the PDFs of the vertical velocity at 2–4 km are narrow,  
417 because the HiCu [project](#) was conducted in the High Plains and the cloud bases ~~are~~ [were](#)

418 relatively high. At 4–6 km, the [observed](#) updrafts become stronger and the PDFs become broader  
419 in all the three field campaigns compared to those at lower levels, especially for COPE and ICE-  
420 T. Above 6 km, the PDFs for the updraft become broader in HiCu while they slightly narrow in  
421 ICE-T compared to those at 4–6 km. For the [observed](#) downdrafts, the PDFs broaden with height  
422 for all the three field campaigns. Generally, the PDFs of the vertical velocity are similar for the  
423 three columns. The main difference is found in the first bins of the vertical velocity (0–2 m s<sup>-1</sup>  
424 and –2–0 m s<sup>-1</sup>): highest for column (a), which includes all the drafts with air mass flux  $\geq 10$  kg  
425 m<sup>-1</sup> s<sup>-1</sup> in magnitude, lowest for column (c), which only includes the strong drafts with air mass  
426 flux  $\geq 500$  kg m<sup>-1</sup> s<sup>-1</sup> in magnitude.

427 In Fig. 8, the [observed](#) updrafts are ~~relatively~~ stronger in ICE-T ~~or~~ [and](#) COPE (maritime or  
428 coastal convective clouds) than in HiCu (pure continental convective clouds). But ~~notice~~ the  
429 aircrafts might under sample the strongest part of the convective cores. In addition, the PDFs are  
430 plotted as a function of MSL height, the relatively narrow PDFs in HiCu compared to COPE and  
431 ICE-T at the same height are possibly because of the higher cloud bases in HiCu. Other than the  
432 ~~sample~~ [sampling](#) issues, the ~~convection~~ triggering mechanism [for convection](#) is also important ~~to~~  
433 [for](#) the updraft strength. The clouds sampled in the three field campaigns are all isolated  
434 convective clouds, the CAPE in HiCu was smaller than in COPE and ICE-T. Compared to [the](#)  
435 GATE project, in which the clouds were also sampled over [a](#) tropical ocean, the PDFs of the  
436 vertical velocity in ICE-T ~~has~~ [have](#) a similar vertical dependence, broadening with height. But  
437 the PDFs are broader in ICE-T than those in GATE, and the maximum vertical velocity (25 m s<sup>-1</sup>)  
438 in ICE-T is greater than that observed in GATE (15 m s<sup>-1</sup>). ~~Notice in~~ [In](#) GATE, the in-situ  
439 measurements also have sampling issues. More measurements are needed to further evaluate the  
440 difference between maritime and continental convective clouds.

441 Fig. 9 shows the PDFs of the air mass flux for all the drafts sampled at 0–2 km, 2–4 km, 4–6 km  
442 and higher than 6 km. The PDFs are exponentially distributed for the three field campaigns at  
443 different heights, which can be fitted using Eq. (1). The coefficients for the fitted function are  
444 shown in each panel. In the three field campaigns, the PDFs of air mass flux have no obvious  
445 trend with height, although the PDFs of diameter and vertical velocity ~~are~~ **broadening** with  
446 height. The differences among the three field campaigns are small for weak and moderate drafts,  
447 and become slightly larger for relatively strong updrafts, which could be due to the sampling  
448 issues.

449

### 450 **4.3 Profiles of vertical velocity and air mass flux**

451 Fig. 10 is a Whisker-Box plot showing the profiles of the vertical velocity (a-c) and air mass flux  
452 (d-f) in the drafts based on the three defined thresholds of air mass flux. The solid box includes  
453 all ~~the~~ three different groups of drafts, the dashed boxes excludes the weak drafts, and the dotted  
454 boxes includes strong drafts ~~only~~. The minimum, 10%, 50%, 90% and ~~the~~ maximum values are  
455 shown in each box. In each panel, the absolute values of the vertical velocities and air mass flux  
456 (except the minimum and maximum ones) are relatively small for the solid boxes.

457 In Fig. 10a-c, the three definitions of drafts show different intensities in the vertical velocities.  
458 Typically, the 10%, 50% and 90% values in the dotted boxes are 1–2 times larger in magnitude  
459 than those in the solid boxes. However, the profiles of the three definitions of drafts vary  
460 similarly with height for each field campaign. In the updrafts sampled during HiCu (Fig. 10a),  
461 the maximum vertical velocity increases with height up to 8 km, then decreases with height

462 above that. The 90% vertical velocity in the solid boxes increases from  $4 \text{ m s}^{-1}$  to  $8 \text{ m s}^{-1}$

463 between 0–10 km. The 10% and 50% vertical velocities in the solid boxes remain similar  
464 between 2–8 km then slightly increase at 8–10 km. In the downdrafts, the minimum vertical  
465 velocity decreases from  $-7 \text{ m s}^{-1}$  to  $-12 \text{ m s}^{-1}$  up to 8 km and increases to  $-9 \text{ m s}^{-1}$  at 8–10 km.  
466 The 10%, 50 % and 90% values all slightly decrease with height. In the updrafts sampled during  
467 COPE (Fig. 10b), the maximum, 10%, 50% and 90% vertical velocities increase with height and;  
468 the observed maximum value is  $23 \text{ m s}^{-1}$ . The minimum vertical velocity in the downdrafts  
469 intensifies from  $-5$  to  $-10 \text{ m s}^{-1}$  with height up to 4 km, then remains similar at 4–6 km. In the  
470 updrafts sampled during ICE-T (Fig. 10c), the maximum vertical velocities increase with height  
471 from  $5.5 \text{ m s}^{-1}$  to  $25 \text{ m s}^{-1}$  up to 6 km, then slightly decreases at 6–8 km. The 90% value increases  
472 from 2 to  $6 \text{ m s}^{-1}$  between 0–4 km, then remains similar at higher levels. The 10% and 50%  
473 values do not show an obvious trend with height. In the downdrafts the minimum vertical  
474 velocity remains similar below 4 km, and decreases to  $-18 \text{ m s}^{-1}$  between 4 km and 8 km. The  
475 10%, 50% and 90% values tend to decrease or remain similar at ~~first~~ lower levels and then  
476 increase with height higher up. The peak ( $\sim 25 \text{ m s}^{-1}$ ) and the minimum ( $\sim -18 \text{ m s}^{-1}$ ) vertical  
477 velocities are observed at 4–6 km and 6–8 km, respectively.

478 To summarize, the observed vertical velocity in the drafts varies differently with height in the  
479 three field campaigns. Stronger downdrafts are often observed in HiCu and COPE compared to  
480 those in ICE-T. The weak, moderate and strong drafts have similar variations with height, but the  
481 magnitudes are the smallest when including all the drafts and become larger if the weak drafts  
482 are excluded. The 10%, 50% and 90% vertical velocities in updrafts and downdrafts over the  
483 tropical ocean (ICE-T) observed in this study generally have similar magnitudes to those shown  
484 in previous studies (e.g. LeMone and Zipser, 1980; Lucas and Zipser, 1994). But strong updrafts  
485 (downdrafts) in excess of  $20 \text{ m s}^{-1}$  ( $-10 \text{ m s}^{-1}$ ) are also observed in this study, which ~~are~~ were



486 rarely reported in previous aircraft observations. This finding is consistent with recent remote  
487 sensing observations (e.g. Heymsfield et al., ~~2009~~2010). The updrafts and downdrafts in  
488 convective clouds over land shown in this study (HiCu) are weaker than those shown by Byers  
489 and Braham (1949) and Heymsfield et al. (~~2009~~2010), possibly because the clouds sampled in  
490 HiCu were isolated convective clouds over ~~high~~High plainsPlains, which ~~could be different~~  
491 ~~than~~apparently differ from deeper convective clouds ~~from~~at lower elevations.

492 Fig. 10d-f shows the profiles the air mass flux statistics for the drafts sampled during the three  
493 field campaigns. As expected, the absolute values of the air mass flux are relatively small if all  
494 the drafts are included (dotted boxes), and become larger if the drafts with relatively small air  
495 mass flux are excluded. However, the variations of the observed air mass flux with height are  
496 similar for the three different definitions in each panel. As determined by the three thresholds,  
497 the minimum absolute values in the solid boxes are about 10 times smaller than those in the  
498 dashed boxes and about 50 times smaller than those in the dotted boxes; ~~for~~For the 10%, 50%,  
499 90% and the maximum absolute values, the differences among the three types of boxes become  
500 smaller. The observed air mass flux varies with height differently for the three field campaigns  
501 and does not have an obvious trend with height. For updraft, the observed maximum air mass  
502 flux is ~~of~~on the order of  $10^4 \text{ kg m}^{-1} \text{ s}^{-1}$ , and the median values for the three different types of  
503 boxes are typically  $\sim 100 \text{ kg m}^{-1} \text{ s}^{-1}$ ,  $\sim 200 \text{ kg m}^{-1} \text{ s}^{-1}$  and  $\sim 1000 \text{ kg m}^{-1} \text{ s}^{-1}$ , respectively. The  
504 observed air mass flux in the downdrafts is a few times smaller in magnitude than those in the  
505 updrafts, but extreme ~~strong~~downdrafts on the order of  $10^4 \text{ kg m}^{-1} \text{ s}^{-1}$  could be observed in some  
506 specific cases. Compared to previous studies, the air mass flux in this study shows similar  
507 magnitudes, but the vertical dependences are different. Lucas and Zipser (1994) shows that the  
508 ~~observed~~convection off tropical Australia ~~intensifies~~intensified with height from 0 to 3 km, then

509 ~~weakens~~weakened with height in terms of air mass flux. Anderson et al. (2005) shows that ~~the~~  
510 ~~observed~~ updrafts and downdrafts over the tropical Pacific Ocean ~~intensify~~intensified with  
511 height up to 4 km, then ~~weakened~~weakened at higher levels. In contrast, this study shows the strongest  
512 updrafts and downdrafts in terms of air mass flux were observed at higher levels.

513

#### 514 4.4 Composite structure of vertical velocity

515 Fig. 11 shows the composite structure for the updrafts and downdrafts with air mass flux  $\geq 10$  kg  
516  $\text{m}^{-1} \text{s}^{-1}$  as a function of normalized scale. The 0 and 1 coordinates on the x-axis indicate the  
517 upwind and downwind sides of ~~the~~the draft, ~~respectively, such that the draft is centered at 0.5.~~  
518 Since we do not have continuous penetrations in a single cloud, we have to statistically analyze  
519 the evolution of the draft structure. In Fig. 11, we can see the normalized shape ~~does not~~do not  
520 ~~have significant~~ change significantly with height, ~~but~~ the observed peak vertical velocity ~~is was~~  
521 ~~strengthening~~does increase with height for all the three field campaigns. If the magnitude of the  
522 vertical velocity is normalized, the structures of the updraft and downdraft at different heights  
523 ~~will~~would be very similar. Connecting this figure to the PDFs of diameter (Fig. 4) and air mass  
524 flux (Fig. 9), the results show statistically ~~that~~that the drafts were expanding (Fig. 4) and the  
525 magnitude of vertical velocity was ~~strengthening~~increasing (Fig. 11), but the air mass flux ~~was~~  
526 ~~not increasing~~remained constant~~has no obvious dependence~~ with height (Fig. 9). This reveals the  
527 complexity of the evolution of the drafts. Based on our datasets, there could be different  
528 possibilities of ~~the~~ updraft changes with height: 1) an updraft ~~expands~~expanded and the vertical  
529 velocity ~~weakens~~weakened with height, 2) an updraft ~~expands~~expanded and the vertical  
530 velocity ~~strengthens~~strengthened with height, 3) an updraft ~~splits~~divided into multiple updrafts

531 and downdrafts, 4) two updrafts merged and ~~become~~became one updrafts. In addition,  
532 entrainment/detrainment and water loading also have important impacts on how drafts change  
533 with height within~~the evolution of drafts in~~ convective clouds.

534 In this composite analysis based on in-situ measurements, the penetration direction has no  
535 obvious impact on the vertical velocity structure, whether the aircraft penetrates along or across  
536 the horizontal wind (not shown). For convective clouds, wind shear has a large impact on the  
537 cloud evolution (Weisman and Klemp 1982); however, the aircraft data are insufficient to reveal  
538 the wind shear impact, because each penetration ~~is~~was made at a single level and the aircraft  
539 ~~does~~did not always penetrate through the center of the draft. Remote sensing data can be helpful  
540 to study the ~~two-dimensional~~2D or ~~three-dimensional~~3D structures of the vertical velocity in  
541 convective clouds. For example, airborne radar with slant and zenith/nadir viewing beams can  
542 ~~provide two-dimensional~~provide 2D wind structure in convective clouds (e.g. Wang and Geerts,  
543 2013). Volumetric radar (e.g. Collis et al. 2013, Jorgensen et al. 2000) can provide ~~three-~~  
544 ~~dimensional~~3D structure of air (or hydrometeor) motion. Thus, in-situ measurements as well as  
545 remote sensing measurements are needed to further analyze the wind shear impact.

546

#### 547 **4.5 Vertical air motion characteristics as clouds evolve**

548 Fig. 12 shows the profiles of ~~the~~-vertical velocity (a-c) and ~~the~~-air mass flux (d-f) for the updraft  
549 and downdraft in the convective clouds with different cloud top heights (CTH). Here, all weak,  
550 moderate and strong updrafts are included. Different colors represent ~~the~~-clouds with different  
551 CTHs. These profiles ~~can~~ generally reveal the change of vertical velocity and air mass flux as the  
552 clouds evolve. The key point presented in Fig. 12a-c is that the peak vertical velocity is observed

553 at higher levels as the clouds evolve. For clouds with CTHs lower than 4 km (red boxes), the  
554 maximum vertical velocity is observed at 2–4 km. When the cloud become deeper, the observed  
555 vertical velocity and air mass flux are stronger at higher levels. ~~This is to be expected, because~~  
556 ~~all the data analyzed in this paper are were collected from isolated convective clouds, so the~~  
557 ~~convective bubbles keep keptcontinue ascending as the clouds evolved. MCSs may have~~  
558 ~~different characteristics of vertical air motion because there is continuous low level~~level  
559 ~~convective source.~~The maximum vertical velocity is observed within 2 km ~~below of~~ below cloud top;  
560 ~~this is~~ consistent with Doppler velocity images measured by WCR (e.g. Fig. 2b) ~~that, which~~  
561 show the ~~typical~~ strongest updraft is typically observed 1–1.5 km below cloud top. The strongest  
562 downdrafts are sometimes observed more than 2 km below cloud top. The 10% and 50% values  
563 do not have obvious trends s as the clouds evolve, possibly because of the increasing contribution  
564 from moderate and weak drafts as the clouds become deeper and broader (Fig. 6 and 7). The  
565 observed air mass flux (Fig. 12d-f) has no obvious trend as the clouds evolve, again suggesting  
566 multiple factors (e.g. entrainment/detrainment, microphysics) ~~have may~~ impact ~~on~~ the evolution  
567 of these se drafts. Since the aircraft ~~just~~ provides ~~a line of the~~ data from just single-line penetrations  
568 ~~through the drafts~~, and not two dimensional2D vertical information, ~~unless the plane it makes~~  
569 ~~multiple passes through the same cell, more~~additional measurements ~~data~~, including remote  
570 sensing measurements are needed to better understand the evolution of the vertical velocity in  
571 convective clouds. ~~at as they go through different stages.~~

572

573 **5. Discussion**

574 In this study, we provide the statistics of vertical air motion in isolated convective clouds using  
575 in-situ measurements from three field campaigns. The statistical results suggest vertical air  
576 motions in convective clouds are very complicated and could be affected by many factors.

577 Microphysics strongly interacts with vertical velocity through different processes, for example,  
578 droplet condensation/evaporation, ice nucleation/sublimation, water loading, etc. Yang et al.  
579 (2016) shows the LWC and IWC are both higher in stronger updrafts in developing convective  
580 clouds, while the liquid fraction has no obvious correlation with vertical velocity. In mature  
581 convective clouds the LWC is also higher in stronger updrafts, but the IWC is similar in  
582 relatively weak and strong updrafts. ~~The~~ liquid fraction is correlated to the vertical velocity  
583 between -3 °C and -8 °C, possibly because Hallet-Mossop process is more significant in weaker  
584 updrafts (Heymsfield and Willis, 2014). Lawson et al. (2015) shows the existence of millimeter  
585 drops in the convective clouds can result in fast ice initiation, and the significant latent heat  
586 released during the ice initiation process can strengthen the updrafts. In ICE-T and COPE, we ~~do~~  
587 also observe many millimeter drops, which may strongly interact with vertical velocity through  
588 fast ice ~~generation~~initiation process. However, in some cases, the existence of millimeter drops  
589 can result in a strong-significant warm rain process (Yang et al. 2016; Leon et al. 2016), which  
590 may weaken the updrafts and ~~make the clouds dissipate quickly~~result in rapid cloud dissipation.

591 Entrainment/detrainment also has a strong interaction with ~~the~~ vertical velocity. In the analysis  
592 above, ~~we see the~~ observed downdrafts observed in HiCu and COPE are ~~obviously~~ stronger than  
593 those observed in ICE-T. This may be partly because the ambient relative humidity is low in  
594 HiCu and COPE compared to ICE-T, resulting in a strong evaporation-cooling effect when the  
595 ambient air ~~mixes~~mixes with cloud parcels through lateral entrainment/detrainment  
596 (Heymsfield et al., 1978). Entrainment has impacts on updrafts as well. Recent ~~study~~studies

597 using in-situ measurements and model simulations suggests stronger entrainment may result in  
598 weaker updrafts (e.g. Lu et al., 2016). In ~~ICE-T~~ [this study](#), we also find ~~the~~ weaker updrafts are  
599 associated with stronger entrainment/detrainment using in-situ measurements of relative  
600 humidity, equivalent potential temperature, droplet concentration and LWC (not shown). ~~In~~  
601 ~~COPE and HiCu, we do not have the appropriate instruments to do similar analyses.~~ Previous  
602 studies (e.g. Heymsfield et al., 1978; Wang et al., 2013) suggest updraft cores unaffected by  
603 entrainment may exist in some convective clouds.

604 Again it is important to be aware of [the](#) limitations of using aircraft in-situ measurements for this  
605 kind of study. More observations (in situ and remote sensing) as well as model simulations are  
606 needed to better characterize the vertical air motion in convective clouds and its interactions with  
607 microphysics and entrainment/detrainment mixing.

608

## 609 **6. Conclusions**

610 The vertical velocity and air mass flux in isolated convective clouds are statistically analyzed in  
611 this study using aircraft data collected from three field campaigns, HiCu, COPE and ICE-T,  
612 conducted over mid-latitude High Plains, mid-latitude coastal area and tropical ocean. Three  
613 thresholds of air mass flux are selected to delineate weak, moderate and strong draft:  $10 \text{ kg m}^{-1} \text{ s}^{-1}$ ,  
614  $100 \text{ kg m}^{-1} \text{ s}^{-1}$  and  $500 \text{ kg m}^{-1} \text{ s}^{-1}$  in magnitude. These definitions only apply for the isolated  
615 convective clouds [analyzed](#) in this study and are not necessarily appropriate for other  
616 convections (e.g. MCSs). The main findings are as follows.

617 1) Small-scale updrafts and downdrafts in convective clouds are often observed in the three  
618 field campaigns. More than 85%, 90% and 74% of the updrafts are narrower than 500 m in HiCu,  
619 COPE and ICE-T, respectively, and more than 90% of the downdrafts are narrower than 500 m  
620 in the three field campaigns combined. These small scale drafts make significant contributions to  
621 the total air mass flux. Updrafts narrower than 500 m contribute 20%–35% of the total upward  
622 flux, and downdrafts narrower than 500 m contribute 50%–65% of the total downward air mass  
623 flux.

624 2) In terms of the air mass flux, the weak and moderate drafts make an important  
625 contribution to the total air mass flux exchange. Generally, the number of drafts increases with  
626 cloud diameter. For many narrow clouds, the weak and moderate drafts dominate and contribute  
627 most of the total air mass flux. For broader clouds, the stronger updrafts contribute most of the  
628 total air mass flux, but the contribution from weak and moderate drafts increases as the cloud  
629 evolves.

630 3) PDFs and profiles of the vertical velocity are provided for the [observed](#) drafts. In all the  
631 height ranges, the PDFs are roughly exponentially distributed and broaden with height. The  
632 [observed](#) downdrafts are stronger in HiCu and COPE compared to ICE-T. Relatively strong  
633 updrafts ( $> 20 \text{ m s}^{-1}$ ) were sampled during ICE-T and COPE. The [observed](#) updrafts in HiCu are  
634 weaker than previous studies of deeper continental convections, possibly because the clouds  
635 sampled in HiCu were isolated convective clouds over [high-High plainsPlains](#), which could be  
636 different than deeper convective clouds from low elevations.

637 4) PDFs and profiles of the air mass flux are provided for the [observed](#) drafts. The PDFs are  
638 similarly exponentially distributed at different heights, and have no obvious trend with height. In

639 the updrafts, the [observed](#) maximum air mass flux has an order of  $10^4 \text{ kg m}^{-1} \text{ s}^{-1}$ . The air mass  
640 flux in the downdrafts are typically a few times smaller in magnitude than those in the updrafts.

641 5) The composite structures of the vertical velocity in the updrafts and downdrafts have  
642 similar normalized shapes for the three field campaigns: the vertical velocity is the strongest near  
643 the center, and weakens towards the edges. Statistically, the vertical velocity and diameter were  
644 increasing with height, but the air mass flux does not have obvious trend with height, suggesting  
645 entrainment/detrainment, water loading and other complicated processes have impacts on the  
646 evolution of the drafts.

647 6) The change of vertical air motion characteristics as the cloud evolves are briefly  
648 discussed. Generally, the strongest portion of a draft ascends with height as the cloud evolves.  
649 The maximum vertical velocity is observed within 2 km below cloud top; the downdrafts are  
650 sometimes stronger at levels more than 2 km below cloud top.

651 The vertical air motion in convective clouds is very complicated, and is affected by many factors,  
652 such as convection mechanisms, entrainment/detrainment and microphysics. This study only  
653 deals with isolated convective clouds and there are ~~several~~[many](#) limitations [of](#) ~~associated with~~  
654 ~~using~~ aircraft in-situ measurements. More data, including [both](#) in-situ and remote sensing  
655 measurements, are needed to better understand the vertical air motion in convective clouds.

656

## 657 **Acknowledgments**

658 This work is supported by National Science Foundation Award: AGS-1230203 and AGS-  
659 1034858, the National Basic Research Program of China under grant no. 2013CB955802 and



660 DOE Grant DE-SC0006974 as part of the ASR program. The authors acknowledge the crew of  
661 NCAR C-130 and University of Wyoming King Air for collecting the data and for providing  
662 high-quality products. Many thanks are also extended to [Drs. Gerald Heymsfield and Scott Collis](#)  
663 ~~the two reviewers~~ for their constructive comments.

664

665 **References**

- 666 Anderson, N. F., Grainger, C. A., and Stith, J. L.: Characteristics of Strong Updrafts in  
667 Precipitation Systems over the Central Tropical Pacific Ocean and in the Amazon. *J. Appl.*  
668 *Meteor.*, 44, 731–738, 2005.
- 669 Arakawa, A.: The cumulus parameterization problem: Past, present, and future. *J. Clim.*, 17,  
670 2493–2525, 2004.
- 671 Bechtold, P., Bazile, E., Guichard, F., Mascart, P. and Richard, E.: A mass-flux convection  
672 scheme for regional and global models. *Quarterly Journal of the Royal Meteorological*  
673 *Society*, 127(573), 869-886, 2001.
- 674 Byers, H. R. and Braham, R. R.: The Thunderstorm-Report of the Thunderstorm Project. U.S.  
675 Weather Bureau, Washington, D.C., Jun 1949. 287 pp. [NTIS PB234515], 1949.
- 676 Collis, S., Protat, A., May, P. T., and Williams, C.: Statistics of Storm Updraft Velocities from  
677 TWP-ICE Including Verification with Profiling Measurements. *J. Appl. Meteor. Climatol.*, 52,  
678 1909–1922, 2013.
- 679 Del Genio, A. D., Wolf, A. B., and Yao, M.-S.: Evaluation of regional cloud feedbacks using  
680 single-column models, *J. Geophys. Res.*, 110, D15S13, doi:10.1029/2004JD005011, 2005.
- 681 Donner, L. J., Seman, C. J., Hemler, R. S., and Fan, S.: A Cumulus Parameterization Including  
682 Mass Fluxes, Convective Vertical Velocities, and Mesoscale Effects: Thermodynamic and  
683 Hydrological Aspects in a General Circulation Model. *J. Climate*, 14, 3444–3463, 2001.

684 Giangrande, S. E., Collis, S., Straka, J., Protat, A., Williams, C. and Krueger, S.: A summary of  
685 convective-core vertical velocity properties using ARM UHF wind profilers in Oklahoma. *J. App.*  
686 *Meteor. Climatol.*, 52, 2278-2295, 2013.

687 Heymsfield, A. J., Johnson, P. N., and Dye, J. E.: Observations of Moist Adiabatic Ascent in  
688 Northeast Colorado Cumulus Congestus Clouds. *J. Atmos. Sci.*, 35, 1689–1703, 1978.

689 Heymsfield, A. J., and Willis, P.: Cloud conditions favoring secondary ice particle production in  
690 tropical maritime convection. *J. Atmos. Sci.*, 71, 4500–4526, 2014.

691 Heymsfield, G. M., Tian, L., Heymsfield, A. J., Li, L., and Guimond, S.: Characteristics of Deep  
692 Tropical and Subtropical Convection from Nadir-Viewing High-Altitude Airborne Doppler  
693 Radar. *J. Atmos. Sci.*, 67, 285–308, 2010.

694 Hildebrand, P. H., Lee, W., Walther, C. A., Frush, C., Randall, M., Loew, E., Neitzel, R., and  
695 Parsons, R.: The ELDORA/ASTRAIA Airborne Doppler Weather Radar: High-Resolution  
696 Observations from TOGA COARE. *Bull. Amer. Meteor. Soc.*, 77, 213–232, 1996

697 Hogan, R. J., Grant, A. L., Illingworth, A. J., Pearson, G. N., and O’Connor, E. J.: Vertical  
698 velocity variance and skewness in clear and cloud-topped boundary layers as revealed by  
699 Doppler lidar, *Q. J. Roy. Meteorol. Soc.*, 135, 635–643, 2009.

700 Houze Jr., R. A., and Betts, A. K.: Convection in GATE, *Rev. Geophys.*, 19(4), 541–576, 1981.

701 Igau, R. C., LeMone, M. A., and Wei, D.: Updraft and Downdraft Cores in TOGA COARE:  
702 Why So Many Buoyant Downdraft Cores?. *J. Atmos. Sci.*, 56, 2232–2245, 1999.

703 Ivanova, I. T. and Leighton, H. G.: Aerosol–Cloud Interactions in a Mesoscale Model. Part I:  
704 Sensitivity to Activation and Collision–Coalescence. *J. Atmos. Sci.*, **65**, 289–308, 2008.

705 Jorgensen, D. P., Zipser, E. J., and LeMone, M. A.: Vertical Motions in Intense Hurricanes. *J.*  
706 *Atmos. Sci.*, **42**, 839–856, 1985.

707 Jorgensen, D. P. and LeMone, M. A.: Vertically Velocity Characteristics of Oceanic Convection.  
708 *J. Atmos. Sci.*, **46**, 621–640, 1989.

709 Jorgensen, D. P., and Smull, B. F.: Mesovortex circulations seen by airborne Doppler radar  
710 within a bow-echo mesoscale convective system. *Bull. Amer. Meteor. Soc.*, **74**, 2146–2157,  
711 1993.

712 Jorgensen, D. P., Shepherd, T. R., and Goldstein, A. S.: A dual-pulse repetition frequency  
713 scheme for mitigating velocity ambiguities of the NOAA P-3 airborne Doppler radar. *J. Atmos.*  
714 *Oceanic Technol.*, **17**, 585–594, 2000.

715 Khairoutdinov, M. F., Krueger, S. K., Moeng, C.-H., Bogenschutz, P. A., and Randall, D. A.:  
716 Large-Eddy Simulation of Maritime Deep Tropical Convection, *J. Adv. Model. Earth Syst.*, **1**, 15,  
717 doi:10.3894/JAMES.2009.1.15, 2009.

718 Khelif, D., Burns, S. P., and Friehe, C. A.: Improved Wind Measurements on Research  
719 Aircraft. *J. Atmos. Oceanic Technol.*, **16**, 860–875, 1999.

720 Kollias, P and Albrecht, B.: Vertical Velocity Statistics in Fair-Weather Cumuli at the ARM  
721 TWP Nauru Climate Research Facility. *J. Climate*, **23**, 6590–6604, 2010.

722 Lawson, P. R., Woods, S., and Morrison, H.: The microphysics of ice and precipitation  
723 development in tropical cumulus clouds. *J. Atmos. Sci.*, 72, 2429-2445, 2015.

724 LeMone, M. A., and Zipser, E. J.: Cumulonimbus vertical velocity events in GATE. Part I:  
725 Diameter, intensity and mass flux. *J. Atmos. Sci.*, 37, 2444–2457, 1980.

726 Leon, D., and co-authors: The CONvective Precipitation Experiment (COPE): Investigating the  
727 origins of heavy precipitation in the southwestern UK. *Bull. Amer. Meteor. Soc.*  
728 doi:10.1175/BAMS-D-14-00157.1, in press, 2016.

729 Lu, C., Liu, Y., Zhang, G. J., Wu, X., Endo, S., Cao, L., Li, Y. and Guo, X.: Improving  
730 parameterization of entrainment rate for shallow convection with aircraft measurements and  
731 large eddy simulation. *J. Atmos. Sci.*, 2015.

732 Lucas, C., Zipser, E. J., and Lemone, M. A.: Vertical Velocity in Oceanic Convection off  
733 Tropical Australia. *J. Atmos. Sci.*, 51, 3183–3193, 1994.

734 May, P. T. and Rajopadhyaya, D. K.: Vertical Velocity Characteristics of Deep Convection over  
735 Darwin, Australia. *Mon. Wea. Rev.*, 127, 1056–1071, 1999.

736 Nicol, J. C., Hogan, R. J., Stein, T. H. M., Hanley, K. E., Clark, P. A., Halliwell, C. E., Lean, H.  
737 W., and Plant, R. S.: Convective updraught evaluation in high-resolution NWP simulations using  
738 single-Doppler radar measurements. *Q. J. R. Meteorol. Soc.*, 141, 3177–3189, 2015.

739 Schmeter, S. M.: Structure of fields of meteorological elements in a cumulonimbus zone, *Hydro.*  
740 *Meteor. Serv., Trans. Cent. Aerol. Obs.* [Trans. From Russian by Israel Prog. For Sci. Trans.,  
741 Jerusalem, 1970, 117 pp.], 1969.

742 Schumacher, C., Stevenson, S. N., and Williams, C. R.: Vertical motions of the tropical  
743 convective cloud spectrum over Darwin, Australia. *Q.J.R. Meteorol. Soc.*. doi: 10.1002/qj.2520,  
744 2015.

745 Tiedtke, M.: A comprehensive mass flux scheme for cumulus parameterization in large-scale  
746 models. *Monthly Weather Review*, 117(8), 1779-1800, 1989.

747 Tonttila, J., O'Connor, E. J., Niemelä, S., Räisänen, P., and Järvinen, H.: Cloud base vertical  
748 velocity statistics: a comparison between an atmospheric mesoscale model and remote sensing  
749 observations. *Atmos. Chem. Phys.*, 11, 9207-9218, 2011.

750 Wang, X., and Zhang M.: Vertical velocity in shallow convection for different plume types, J.  
751 *Adv. Model. Earth Syst.*, 6, 478–489, 2014.

752 Wang, Y. and Geerts, B.: Composite Vertical Structure of Vertical Velocity in Nonprecipitating  
753 Cumulus Clouds. *Mon. Wea. Rev.*, 141, 1673–1692, 2013.

754 Wang, Z. and co-authors: Single aircraft integration of remote sensing and in situ sampling for  
755 the study of cloud microphysics and dynamics. *Bull. Amer. Meteor. Soc.*, 93, 653–668, 2012.

756 Weisman, M. L. and Klemp, J. B.: The dependence of numerically simulated convective storms  
757 on vertical wind shear and buoyancy. *Monthly Weather Review*, 110, 504-520, 1982.

758 Wendisch, M., and Brenguier, J.: *Airborne Measurements for Environmental Research: Methods*  
759 *and Instruments*. Wiley, 520 pages, 2013.

760 Wu, J., Del Genio, A. D., Yao, M.-S., and Wolf, A. B.: WRF and GISS SCM simulations of  
761 convective updraft properties during TWP-ICE, *J. Geophys. Res.*, 114, D04206,  
762 doi:10.1029/2008JD010851, 2009.

763 Yang, J., Wang, Z., Heymsfield, A. J., and Luo, T.: Liquid/Ice Mass Partition in Tropical  
764 Maritime Convective Clouds. *J. Atmos. Sci.*, in review, 2016.

765 Zipser, E. J., Cecil, D. J., Liu, C., Nesbitt, S. W., and Yorty, D. P.: Where are the most intense  
766 thunderstorms on Earth?. *Bull. Amer. Meteor. Soc.*, 87, 1057–1071, 2006.

767

Table 1. Number of penetrations, time in clouds and flight length in clouds sampled at 0–2 km, 2–4 km, 4–6 km, 6–8 km and 8–10 km MSL in HiCu, COPE and ICE-T.

Height (km MSL)	HiCu			COPE			ICE-T		
	Number of penetrations	Time in clouds (min)	Length in clouds (km)	Number of penetrations	Time in clouds (min)	Length in clouds (km)	Number of penetrations	Time in clouds (min)	Length in clouds (km)
8–10	43	12	79						
6–8	565	122	789				132	52	423
4–6	596	104	653	207	39	244	299	116	895
2–4	373	50	274	378	86	486	34	10	73
0–2				219	40	211	197	27	167



Table 2. Number of updrafts and downdrafts sampled at 0-2 km, 2-4 km, 4-6 km, 6-8 km and 8-10 km in HiCu, COPE and ICE-T.

Three numbers are given for the updraft and downdraft at each level, respectively, according to the three different definitions: weak, moderate and strong.

Height (km)		HiCu		COPE		ICE-T	
		Updraft	Downdraft	Updraft	Downdraft	Updraft	Downdraft
8-10	weak	66	100				
	moderate	52	44				
	strong	44	17				
6-8	weak	818	763			382	372
	moderate	559	540			175	136
	strong	287	130			102	23
4-6	weak	748	668	290	184	858	671
	moderate	522	389	232	193	425	329
	strong	343	48	135	51	266	73
2-4	weak	311	235	568	424	49	47
	moderate	271	84	467	434	51	51
	strong	149	7	188	101	32	10
0-2	weak			368	192	319	205
	moderate			266	90	234	104
	strong			96	9	60	7

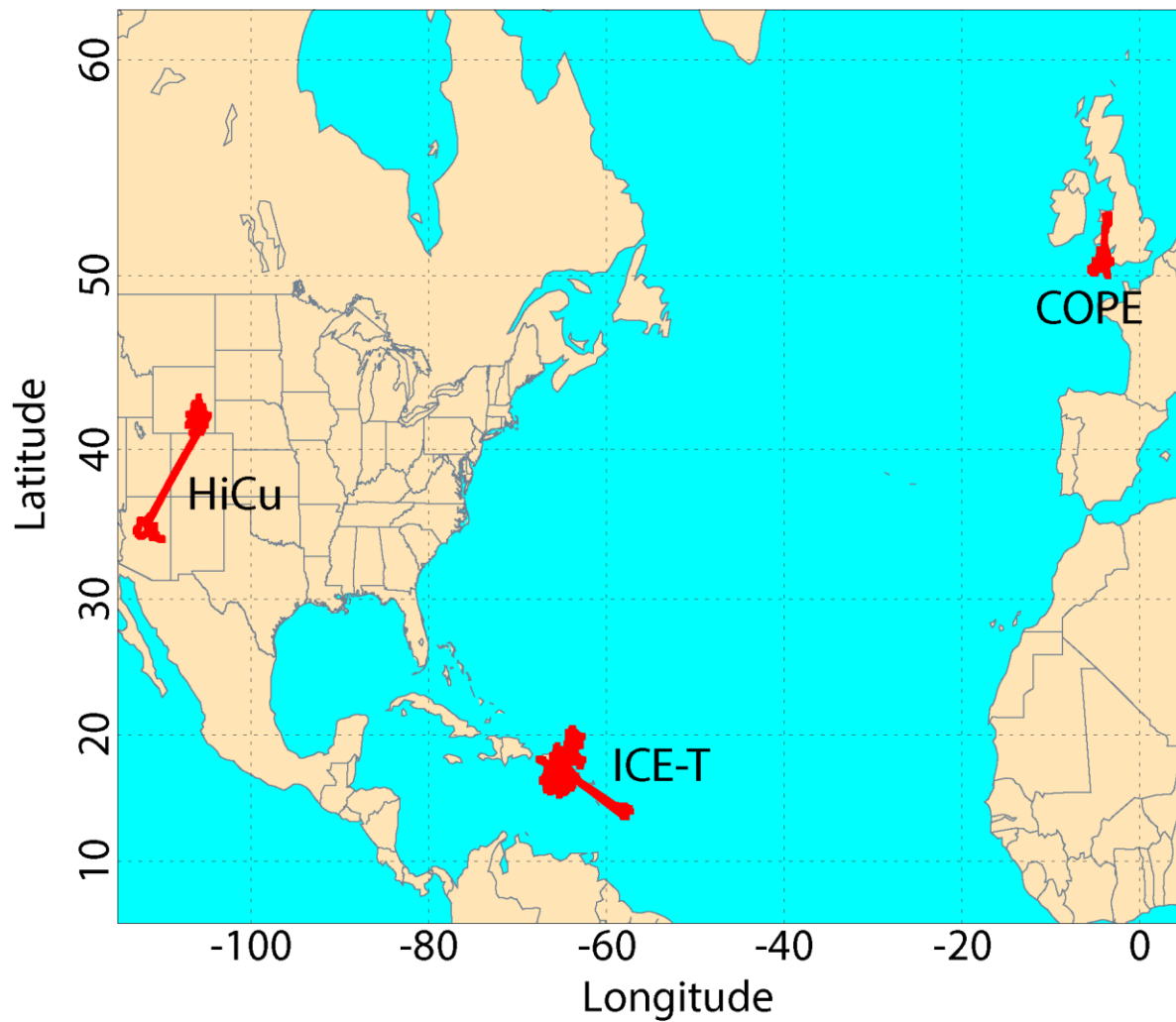


Figure 1. Flight tracks for the three field campaigns: HiCu, COPE and ICE-T.

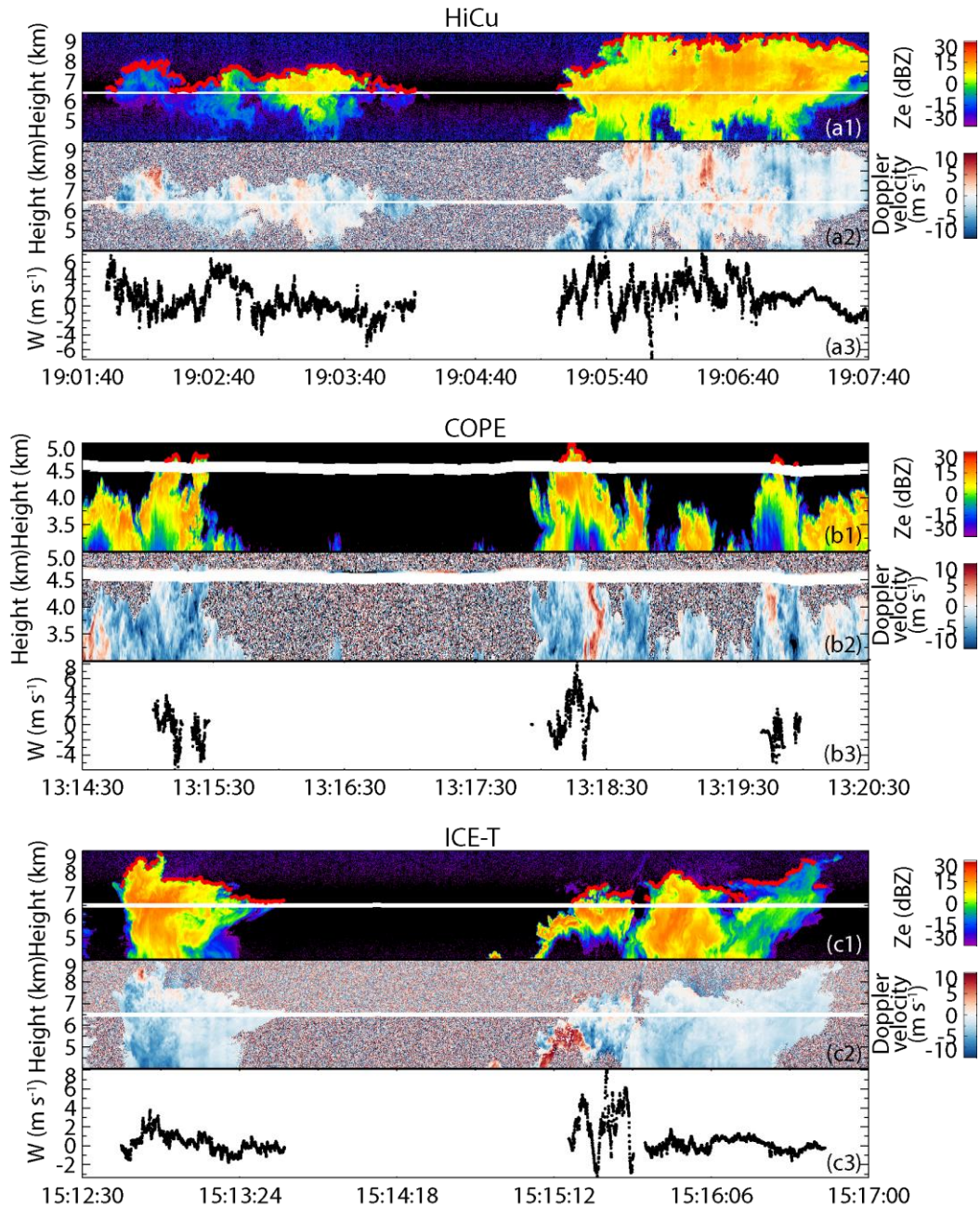


Figure 2. Examples of radar reflectivity, Doppler velocity and 25-Hz in-situ vertical velocity measurements for the convective clouds sampled in HiCu, COPE and ICE-T. The red dots in (a1), (b1) and (c1) are the cloud tops estimated by WCR.

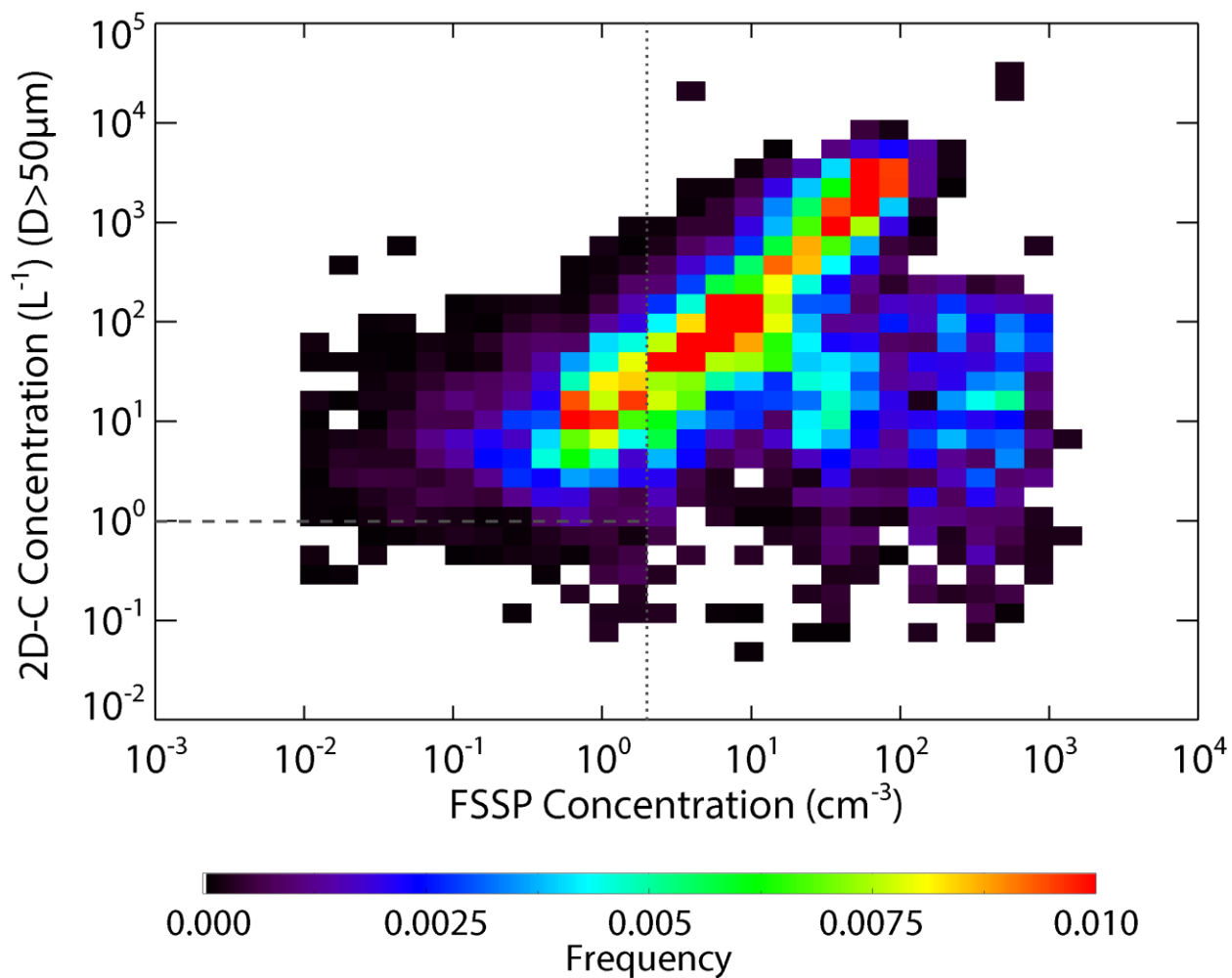


Figure 3. Occurrence distributions as a function of the particle concentrations measured by FSSP versus the concentrations of the particles  $\geq 50 \mu\text{m}$  in diameter measured by 2D-C in the clouds identified by WCR reflectivity. The dashed and dotted lines indicate the FSSP concentration equal  $2 \text{ cm}^{-3}$  and the 2D-C concentration equal  $1 \text{ L}^{-1}$ , respectively.

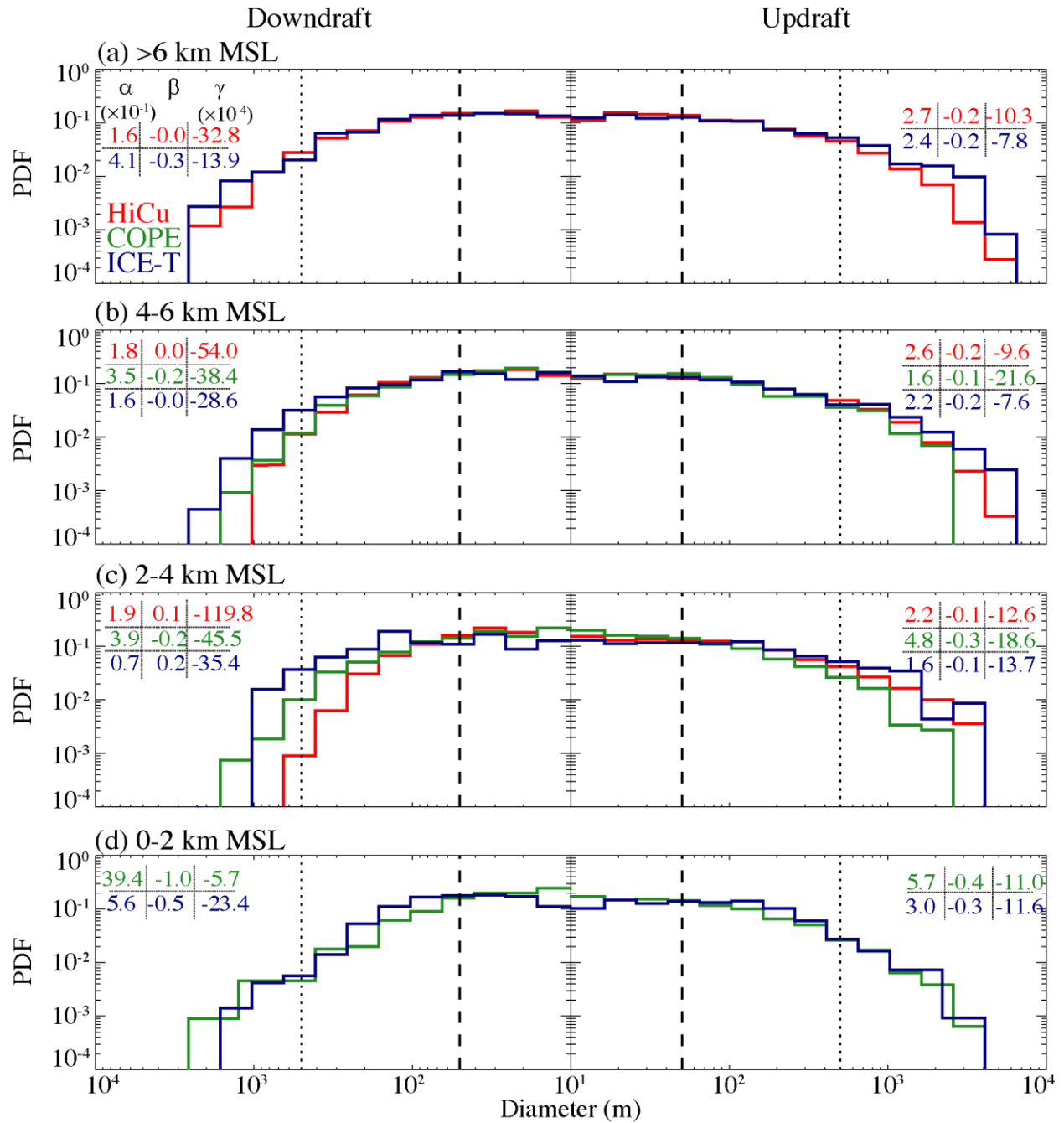


Figure 4. PDFs of the diameters for the updrafts and downdrafts sampled at 0–2 km, 2–4 km, 4–6 km and higher than 6 km. The numbers shown in each panel are the coefficients of the fitted exponential function (Eq. 1).

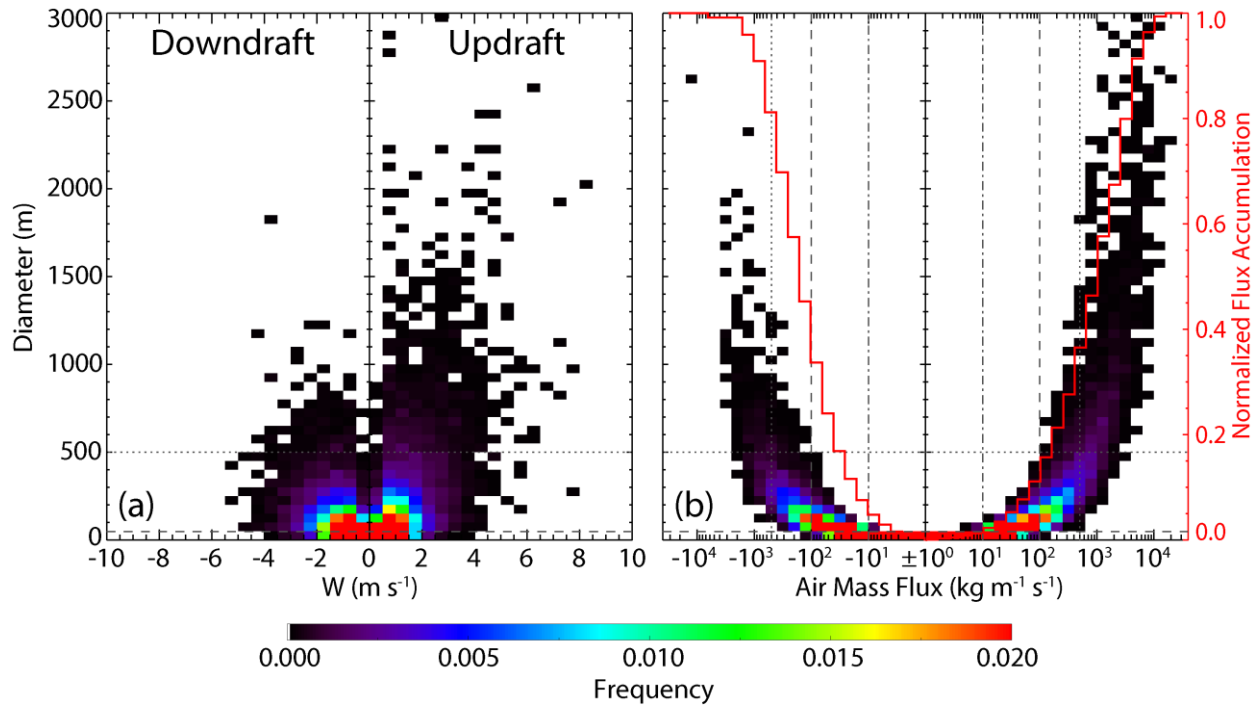


Figure 5. Occurrence distributions as (a) a function of diameter and mean vertical velocity, and (b) a function of diameter and air mass flux for all updrafts and downdrafts. The normalized accumulation flux is also shown by the red curves. The horizontal dotted and dashed lines in (a) and (b) indicate the draft diameter equal 500 m and 50 m, which are used as the diameter thresholds to identify a “draft” in previous studies and in this study, respectively. The vertical dash-dotted, dashed and dotted lines in (b) indicate air mass flux equal  $10 \text{ kg m}^{-1} \text{s}^{-1}$ ,  $100 \text{ kg m}^{-1} \text{s}^{-1}$  and  $500 \text{ kg m}^{-1} \text{s}^{-1}$  in magnitude, respectively, which are the thresholds used to delineate the three different groups of draft.

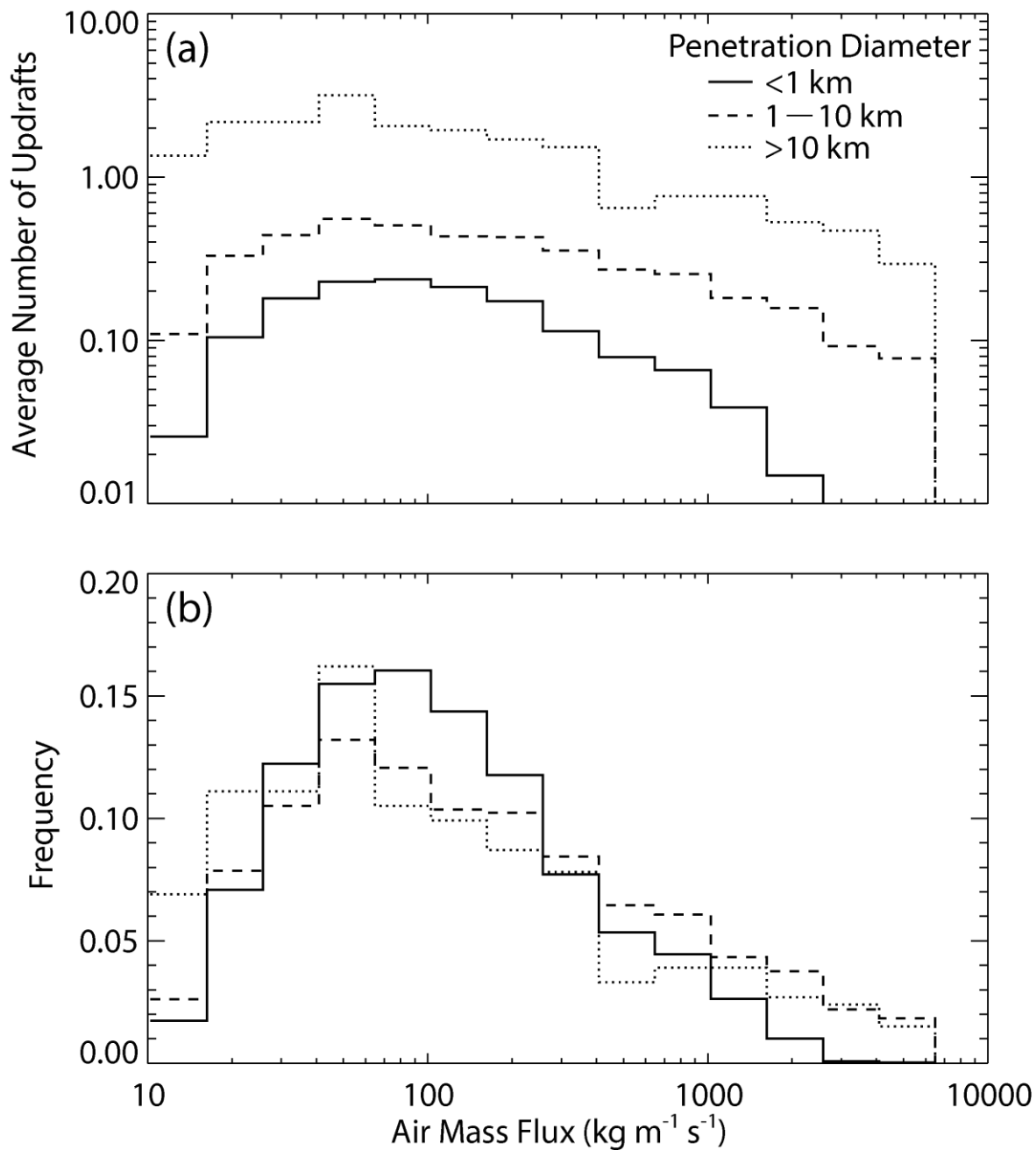


Figure 6. (a) Average number and (b) occurrence frequency of updrafts as a function of air mass flux observed in penetrations with length < 1 km (solid), 1-10 km (dashed) and >10 km (dotted).

The result is a composite of HiCu, COPE and ICE-T.

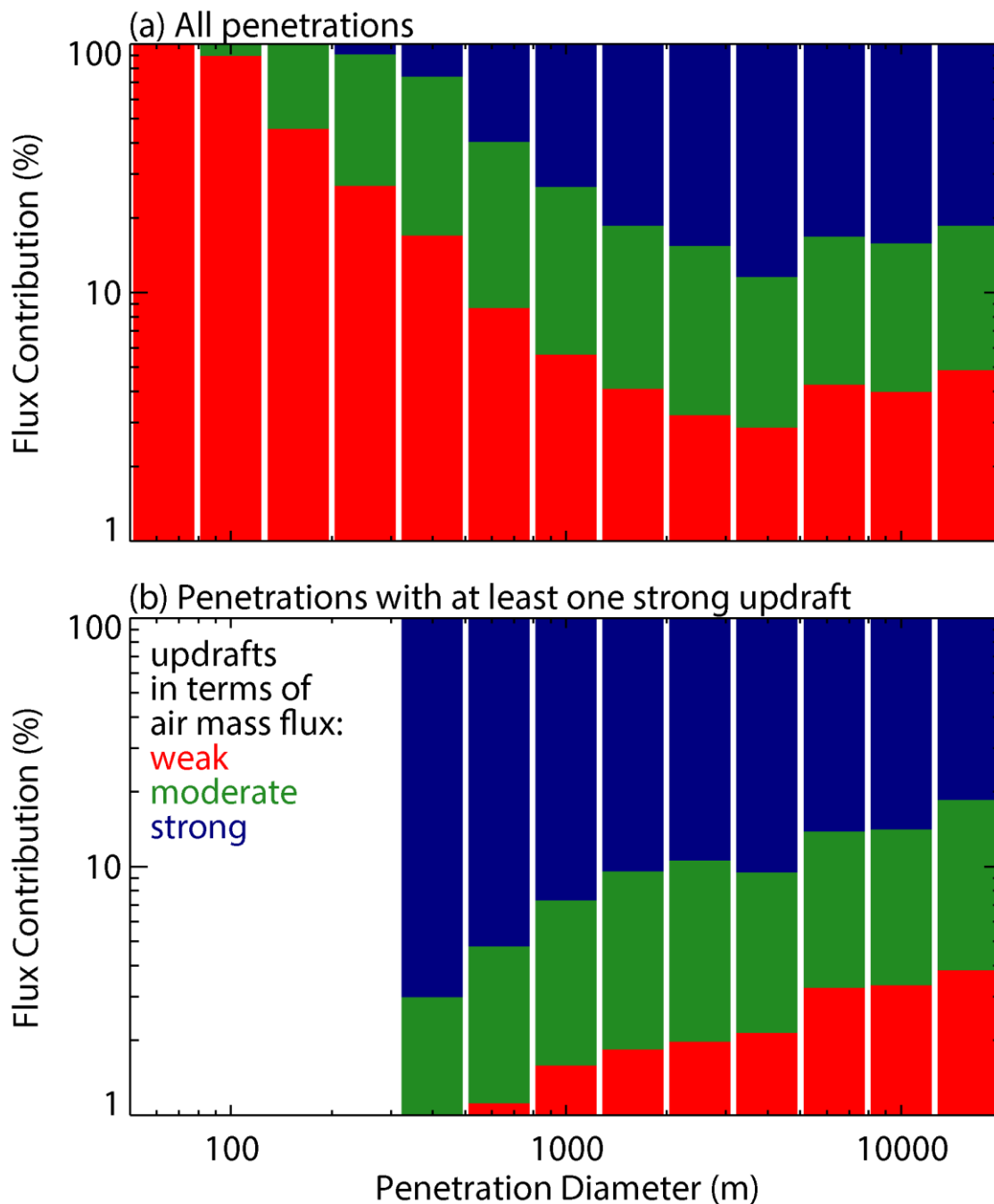


Figure 7. Average percentile contribution to total upward air mass flux by the weak (red), moderate (green) and strong (blue) updrafts delineated in this study. The result is a composite of HiCu, COPE and ICE-T.



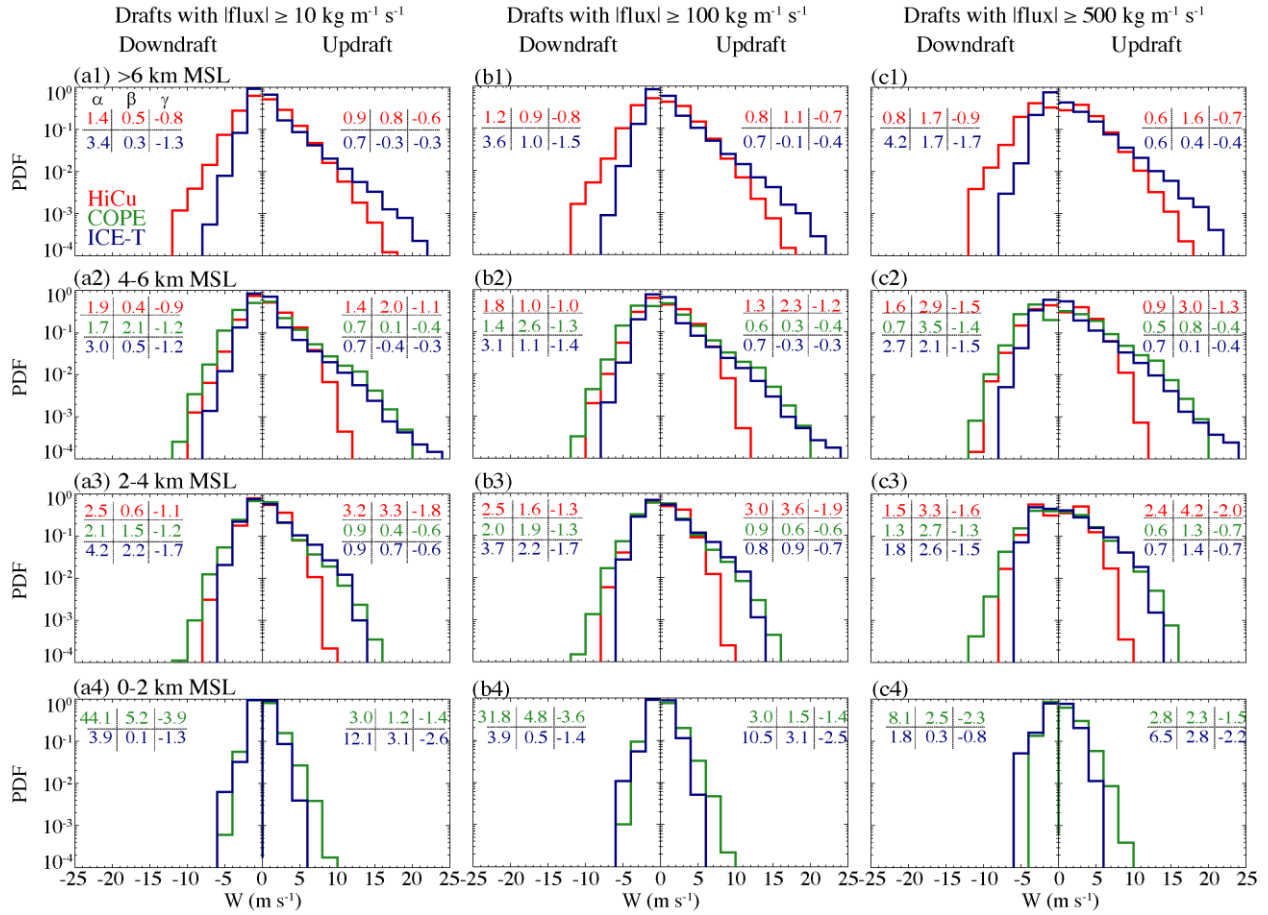


Figure 8. PDFs of the 25-Hz vertical velocity for the updrafts and downdrafts with air mass flux  $\geq$  (a)  $10 \text{ kg m}^{-1} \text{ s}^{-1}$ , (b)  $100 \text{ kg m}^{-1} \text{ s}^{-1}$  and (c)  $500 \text{ kg m}^{-1} \text{ s}^{-1}$  in magnitude, sampled at 0–2 km, 2–4 km, 4–6 km and higher than 6 km. The numbers shown in each panel are the coefficients of the fitted exponential function (Eq. 1).

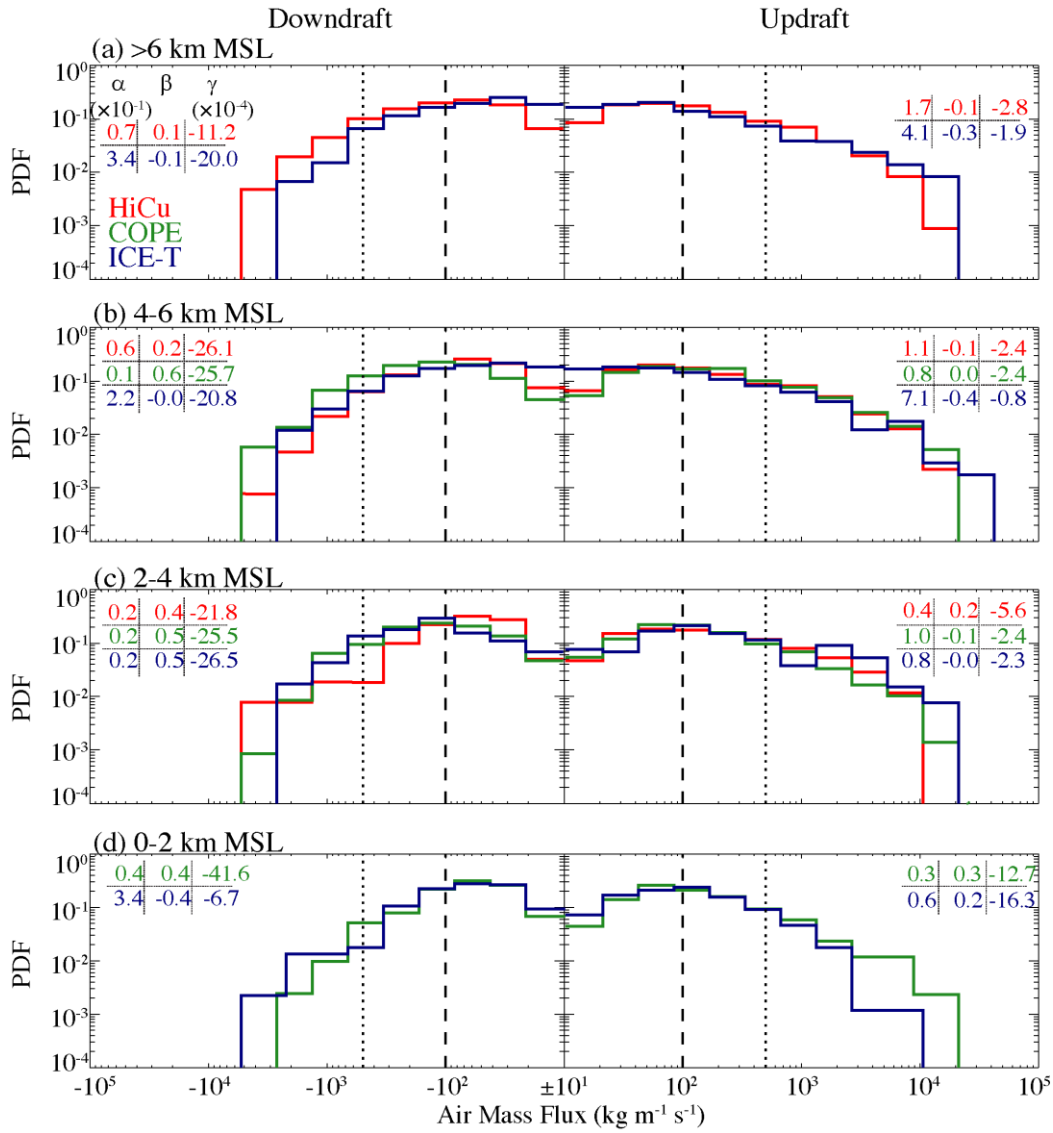


Figure 9. PDFs of the air mass flux for the updrafts and downdrafts sampled at 0–2 km, 2–4 km, 4–6 km and higher than 6 km. The three thresholds of the air mass flux ( $\pm 10$   $\text{kg m}^{-1} \text{s}^{-1}$ ,  $\pm 100$   $\text{kg m}^{-1} \text{s}^{-1}$  and  $\pm 500$   $\text{kg m}^{-1} \text{s}^{-1}$ ) are shown by the solid (overlaps with the central y-axis in each panel), dashed and dotted lines. The numbers shown in each panel are the coefficients of the fitted exponential function (Eq. 1).

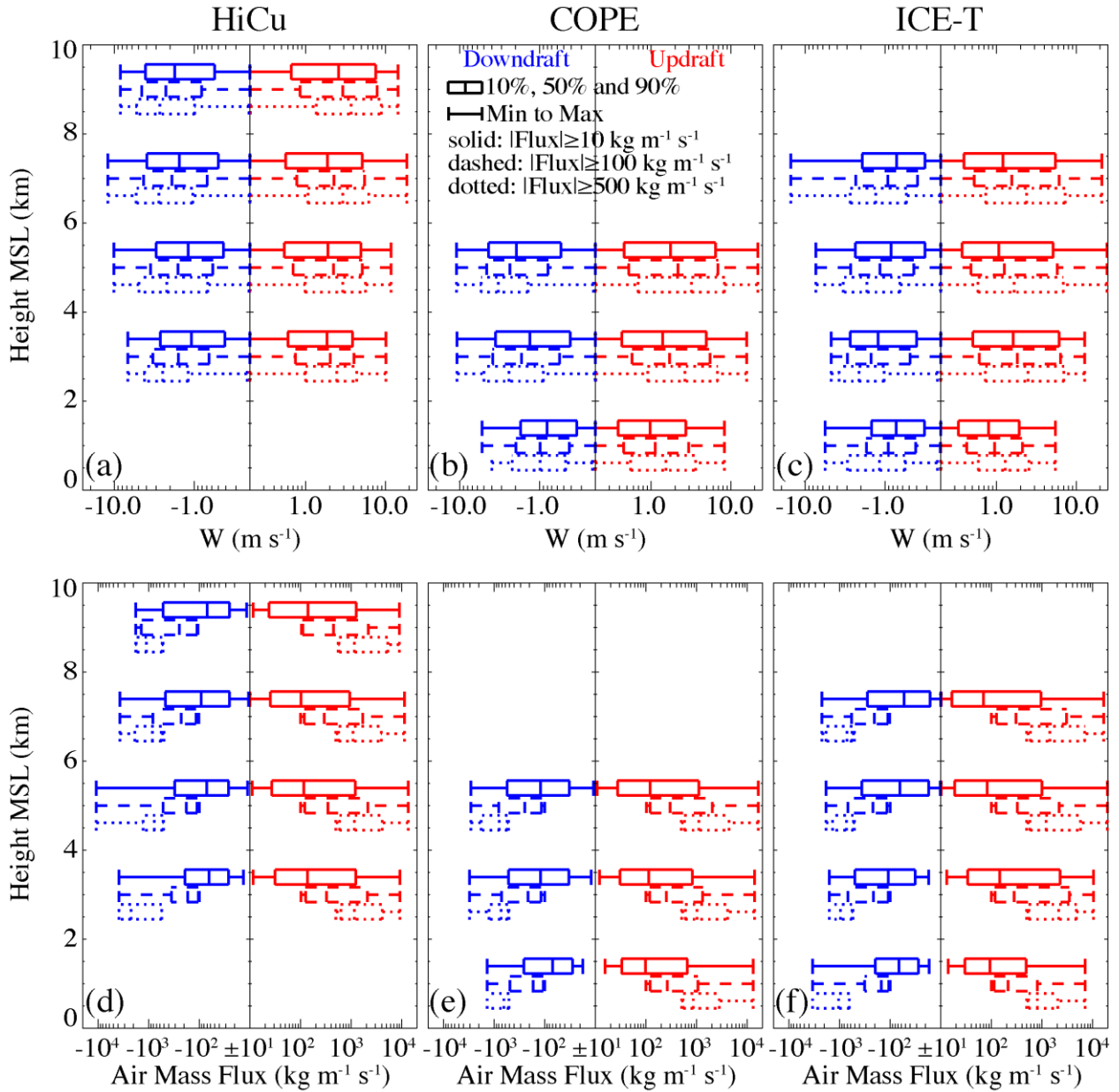


Figure 10. Profiles of (a-c) the vertical velocity and (d-f) air mass flux for all the updrafts and downdrafts sampled at 0–2 km, 2–4 km, 4–6 km, 6–8 km and 8–10 km. The dotted, dashed and solid boxes represent for the drafts with air mass flux  $\geq 10 \text{ kg m}^{-1} \text{ s}^{-1}$ ,  $100 \text{ kg m}^{-1} \text{ s}^{-1}$  and  $500 \text{ kg m}^{-1} \text{ s}^{-1}$  in magnitude, respectively.

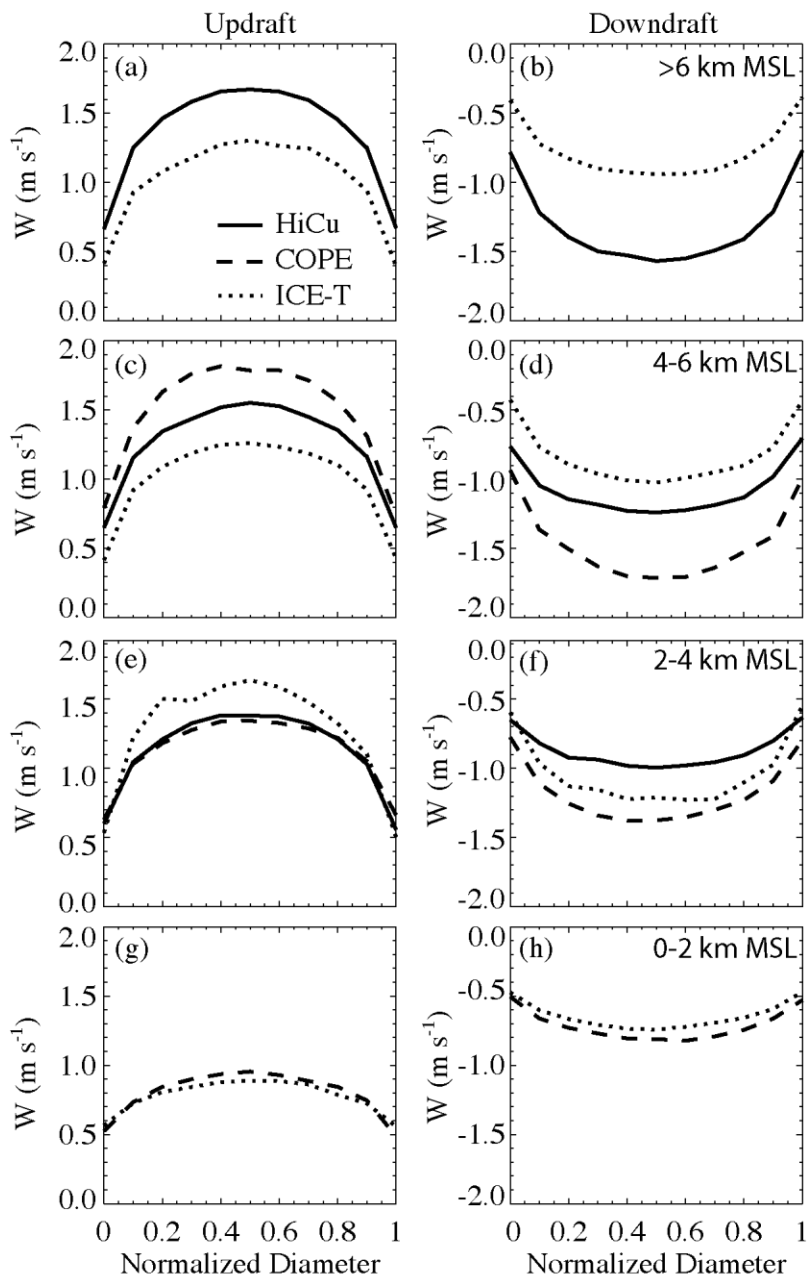


Figure 11. Composite structure of the vertical velocity as a function of the normalized diameter for the updrafts and downdrafts with air mass flux  $\geq 10 \text{ kg m}^{-1} \text{ s}^{-1}$  in magnitude. The 0 and 1 coordinates on the x-axis indicate the upwind and downwind sides of the draft.

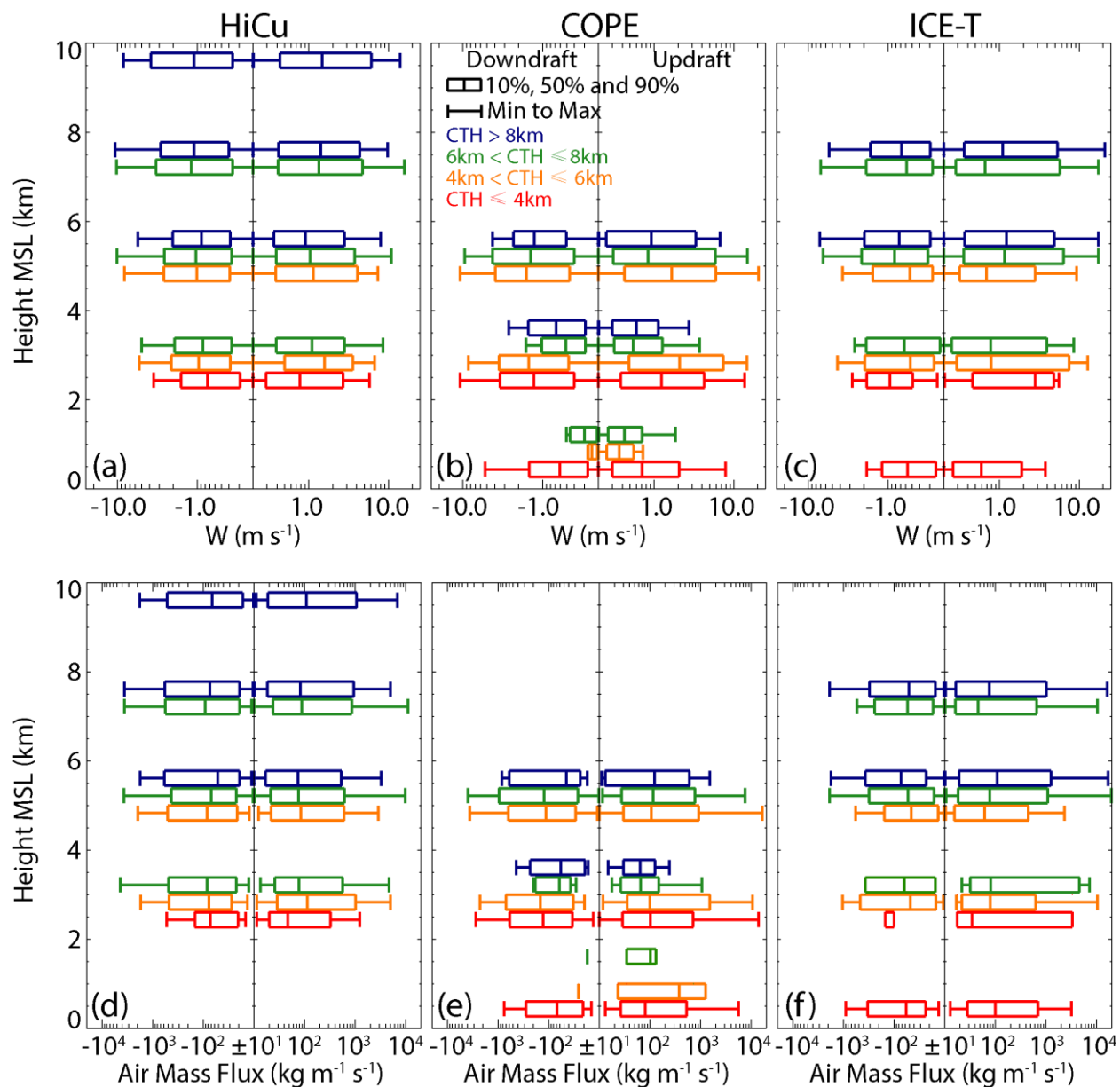


Figure 12. Profiles of (a-c) the vertical velocity and (d-f) the air mass flux for the updraft and downdraft with air mass flux  $\geq 10 \text{ kg m}^{-1} \text{ s}^{-1}$  in magnitude. The red, orange, green and blue boxes represent clouds with cloud top heights of 0-4 km, 4-6 km, 6-8 km and higher than 8 km.